

POLITECNICO DI TORINO

Master Degree in Mechanical Engineering
Department of Mechanical and Aerospace Engineering



Master thesis

**Rigid and flexible 3D models for rotors
with passive magnetic supports**

Supervisors:

Prof. Alessandro Vigliani

Prof. Elvio Bonisoli

Ing. Domenico Lisitano

Candidate:

Eleonora Guelfi

243168

Anno Accademico 2018 - 2019

“E quindi uscimmo a riveder le stelle.”

Dante, Inferno XXXIV

Contents

Abstract	9
Introduction	11
Chapter1	11
1 Overview on rotordynamics	13
1.1 History of rotordynamics	15
1.2 Stability of a rotating structure	19
1.3 Stability of a magnetic structure	21
Chapter2	22
2 Finite element model	23
2.1 Rod element	23
2.1.1 Euler-Bernoulli rod element	27
2.1.2 Timoshenko rod element	30
2.2 Assembly of the structure	33
2.2.1 From local to global reference frame	33
2.2.2 Application of the constraints	35
2.3 Gyroscopic formulation	36
2.3.1 Conservative and real matrices	36
2.3.2 Classical dissipative and real matrices	39
Chapter3	41
3 Testbench	43

3.1	Description of the parametric test-rig	43
3.1.1	Inertial properties	45
3.1.2	Magnetic supports	47
3.2	3D finite element model	48
Chapter4		51
4	Numerical results	53
4.1	Rigid model	53
4.2	Flexible model	56
4.3	Comparison	60
Conclusions		62
Reference		65

List of Figures

1.1	Rotor whirling at speed ω and spinning at speed Ω [1].	14
1.1.1	Jeffcott rotor: isometric view (left), orthogonal view (right) [6].	16
1.2.1	Forward and backward modes (left) and stability of a rotor (right) [25].	21
2.1.1	Rod in a local reference frame	24
2.1.2	Rods with solid (a) and annular (b) cross-section [27].	24
2.1.3	Effect of shear deformation on bending for Euler Bernoulli beam (a) and Timoshenko beam (b) [1].	26
2.1.1.1	Rod cross-section parameters [27].	29
2.2.1.1	Assembling of global matrices [29].	34
3.1.1	Model of vertical magnetic rotor.	43
3.1.2	Rotor with four hubs and six magnets.	45
3.1.1.1	Particular of a brass hub.	46
3.1.2.1	Particular of magnetic rings.	47
3.2.1	3D model of the rotor on magnetic supports.	48
3.2.2	Nodes of the discretised rigid shaft and barycentre G.	49
4.1.1	Conical modes at low frequency.	54
4.1.2	Bounce modes at $S = 9.143$ Hz.	54
4.1.3	Bounce modes at $S = 9.168$ Hz.	54
4.1.4	Conical modes at high frequency.	55
4.1.5	Shaking modes.	55
4.1.6	Rigid body modes.	56
4.2.1	Nodes of the discretised flexible shaft and barycentre G.	57

4.2.2	First flexible modes at $S = 482.2$ Hz.	58
4.2.3	First flexible modes at $S = 482.6$ Hz.	58
4.2.4	First flexible modes at $S = 483$ Hz.	58
4.2.5	Second flexible modes at $S = 607.9$ Hz.	59
4.3.1	4 degrees of freedom rotor [1] (a) and 3D rigid model (b).	60
4.3.2	(a) 3D rigid model and (b) 3D flexible model.	61
4.3.3	Stability for the rigid (a) and flexible (b) rotor.	62

List of Tables

2.1.1	Generalized DOF and behaviour	24
3.1.1	Characteristics of the rotor in the chosen configuration.	45
3.1.1.1	Hub geometric and material characteristics.	46
3.1.2.1	Geometric and material characteristics of the rings.	47

Abstract

The aim of this thesis is the 3D rotordynamic analysis of a flywheel with passive magnetic supports. The thesis is developed starting from a rigid body model and its relative Campbell diagram is analysed in real coordinates. The already known simulation result can be generalised by formulating a 3D finite elements analysis, building the elementary matrices of a cylindrical rod to study the gyroscopic behaviour in conservative and dissipative systems, with related computations of eigenvalues and eigenvectors. A 3D FEM rotordynamic model is developed based on an existing device, previously designed and built, of a parametric test-rig (variable rotating mass) on passive magnetic supports with minimum resistance to rotation. The model is built with a real coordinates approach of flexible rotordynamics. A comparison between the predictions for the rigid and the 3D flexible models is proposed using parametric analysis and Campbell diagrams. The numerical results assess the method robustness and the feasibility to pass in simulation from a rigid to a rigid-flexible behaviour. This model is suitable to provide a prediction for the next step of experimental validation on the parametric test-rig.

Introduction

The discipline concerning rotors has been intensely studied in the last century, in particular after World War II when aeronautical turbines were developed. With the advent of computers, the study of this subject has been extended to complex rotors, this thanks to the computational power available. An overview of the researches performed in this field, which have given a contribution to the actual knowledge, is presented in the first part of Chapter 1. Then, the discussion proceeds on the stability criterion for a rotating structure on magnetic supports. Chapter 2 is focused on the analysis of a rotating structure using the Finite Element Method. The rod element, used to discretise the assembly, is presented and the formulation of its elementary matrices with Euler-Bernoulli and Timoshenko approach are reported. The procedure followed to build the global matrices of the structure and the application of the proper constraints is explained. The method to solve the eigenproblem, both for a conservative and classical dissipative structure, with the Duncan formulation, is proposed at the conclusion of the section. The parametric test bench is presented in Chapter 3, where particular attention is given to the variable mass components and the passive magnetic bearings. It follows the description of the 3D discretised model built with FEM and the presentation of its related matrices. Chapter 4 starts showing the modes of the 3D rigid model, that have been derived from the analysis previously explained. Then, a comparison of the Campbell diagram of the rigid model with the four degrees of freedom rotor described in literature is reported. Since the rigid model results to be reliable, a flexible model of the rotor is then presented. In conclusion, the Campbell diagrams for the 3D FE rigid and flexible model are reported and their stability discussed. Conclusions and next steps of the project are, finally, stated and discussed.

Chapter 1

Overview on rotordynamics

Rotordynamics is a specialised branch of applied mechanics dealing with the study of the behaviour and diagnosis of rotors, mechanical devices, eventually supported by bearings or hinges, which rotate about a fixed axis. At the design stage of any rotating machine, a rotordynamic analysis is required to predict the possible dynamic problems. During testing, it is used to compare the experimental results with the theoretical behaviour and it is very important for balancing procedures and diagnostics.

In a plant, it is possible to distinguish rotating components and static ones: the part of the machine that does not rotate is called stator. Rotors constrained with bearings to spin around a fixed axis are referred to as fixed rotors, whereas those that are not constrained in any way are defined free rotors. This general definition states that, aside from the artificial rotors built by human technology, rotordynamics is able to describe the behaviour of natural rotors, such as spinning celestial bodies.

In the field of mechanics, rotating systems such as turbines, jet engines have to be studied, so the attention is mainly focused on fixed rotors. These devices are unbalanced: due to manufacturer precision, for which the centre of rotation never coincides with the barycentre (*static unbalance*), or due to mounting errors, for which the principal axis of inertia is not coinciding with the rotation axis (*dynamic unbalance*). Usually both the situations come into play, so the expression *couple unbalance* is used. Unbalanced rotors experience two types of rotation: they spin about their axis and whirl about the deformed axis line, this second motion is called *precession*.

The study of rotors is focused on the precession, which is a form of vibration analogous

to the oscillating phenomena occurring in static structures. The main difference holds in the fact that when vibration is produced in a rotating structure, it is transported from the spinning motion, thus resulting in an overlapping of rotation and vibration, which shows itself as a precession. Depending on the properties of the structure and the excitation, it is possible to identify different kind of precession: cylindrical or conical trajectory, forward or backward and synchronous or asynchronous way of rotation with respect to spinning.

An example of a simple model of a rotating shaft on isotropic supports, showing forward synchronous whirling motion, is shown in Figure (1.1):

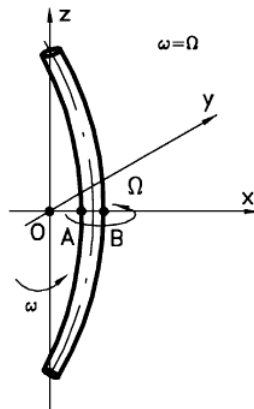


Figure 1.1: Rotor whirling at speed ω and spinning at speed Ω [1].

Similarly to a static structure, a rotating one is characterized by some natural frequencies, representing the whirling motion, that can be determined analysing the eigenvalue problem and have the particularity to depend on the spin speed. The orbit of the rotor changes according to its natural frequencies, so for any rotor it can be defined a *critical speed*, at which corresponds the maxima of the trajectory, and the *threshold of instability*, speed at which the orbit starts growing exponentially. Once determined the properties of the rotating structure and the external excitations applied on it, analytical procedures can be adopted to determine these parameters, fundamental information to study the behaviour of the rotor in operating conditions.

1.1 History of rotordynamics

The starting point in the study of rotors is commonly dated in 1869 when Rankine delivered to the scientific community his work “On The Centrifugal Force of Rotating Shafts” [2]. In this publication, the author introduced the concept of critical speed for a rotating structure, such as the speed at which the rotor experiences large amplitude vibrations. Moreover, he wrongly stated the impossibility to run the machine beyond the critical speed without experiencing its failure.

This assertion was invalidated in 1895, when De Laval experimentally demonstrated that a turbine can operate in the supercritical range.

In the meanwhile, the studies of Dunkerley [3] and Föppl [4], gave important results: it was discovered that a rotor, depending on its size, elasticity and supports, may have more than one critical speed. Nevertheless, it was determined the existence of some critical speeds equal to the natural frequencies of a non rotating system with the same properties. In particular, Föppl’s work, demonstrated the behaviour of a two degrees of freedom model of rotor, but this did not have relevance in the following few years.

In 1919, Jeffcott [5] proposed the first model of a rotor that could be studied with a lumped parameters approach. Also known as De Laval rotor, it consists of an axial-symmetric isotropic disc, rotating on a massless shaft, supported by axial-symmetric isotropic bearings, shown in Figure (1.1.1). The disc is analysed reducing it to a point mass only excited by the elastic restoring force of the shaft. This model is useful to explain some characteristic phenomena of rotors: the growing of the orbit in correspondence to a critical speed and the self-centring of the disc in the supercritical field. On the other hand, this model does not approximate very well the behaviour of real rotors. A further step in this domain was obtained with the introduction of the four degrees of freedom rotor model, which is basically a Jeffcott rotor where the disc is assumed to be a rigid body. A rigid body has six degrees of freedom in space, but this model reduces them to four because it does not consider the axial and torsional behaviour. This assumption does not lead to a loss of generality, since the main phenomena taking place in rotating systems, differently from translational systems, are of flexural nature.

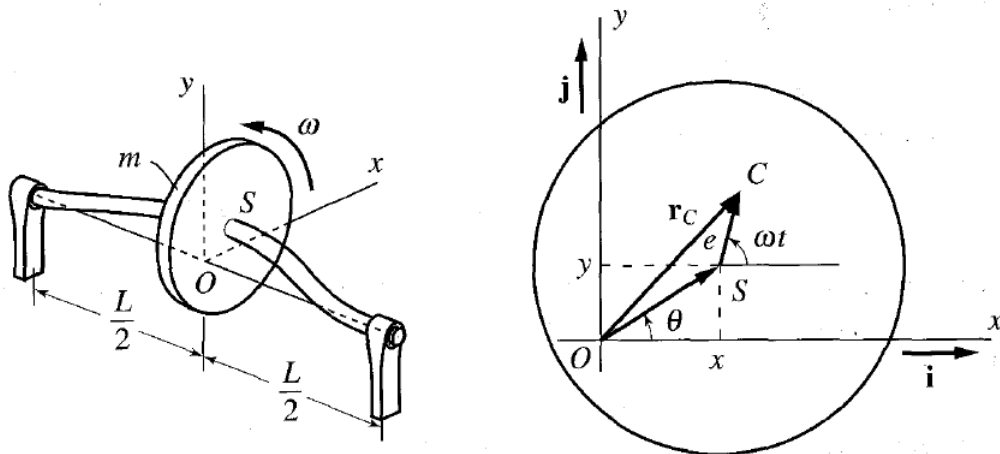


Figure 1.1.1: Jeffcott rotor: isometric view (left), orthogonal view (right) [6].

Thus, this model is able to provide a more realistic analysis with respect to the Jeffcott rotor, because it takes into account the presence of the moments of inertia of the structure and their effect on the dynamic behaviour. In particular, they can produce gyroscopic effects, which play an important role in flexural vibrations, causing the natural frequencies of bending modes to depend on the spin speed of the rotor. Referring to a principal reference system, the moments of inertia of the rotor are the polar moment of inertia about the rotating axis, usually called J_p , and the transversal moment of inertia about any axis in the rotation plane, usually called J_t . Structures where $J_p > J_t$ are referred to as discs, on the contrary if it holds $J_p < J_t$ they are called long rotors. In the particular case of $J_p = J_t$, the ellipsoid of inertia becomes a sphere and this situation is similar to the Jeffcott rotor model.

For what concerns complex rotors, multi degrees of freedom models are required and generally they can be described with cylindrical rod elements. The dynamic evolution of this element, dependent on axial, torsional and flexural behaviour, is described with partial differential equations, which can be directly solved only for easy shapes and under some boundary conditions.

Moreover, the equations of motion are formulated under some assumptions related to the geometry of the model. The two main approaches are the Euler-Bernoulli beam theory, which dates back to 1750, and the Timoshenko theory, presented in 1921 [7].

As it is well known, the first one is a particular case of the second because it does not consider the shear effect due to the deformation. The validity of this assumption depends on the geometry of the rotor: for long rotors the shear effect is negligible with respect to the flexural behaviour of the structure, while for discs it has an important impact. It could be stated that in general one theory is not better than the other, therefore the one that better model the rotor should be used.

Since the continuum approach leads to problems in the analytical solutions, numerical techniques have been adopted. Different approaches have been applied: first the reduction of the structures to a numerical model to find the analytical solution has led to some results, but general cases can only be faced using discretisation methods.

Fundamental contributions to the topic have been given in 1944 by Nils Otto Myklestad [8], who developed a technique for the dynamic study of a cantilever aircraft wing. Later in 1945, Prohl [9] extended the formulation to rotating systems including also gyroscopic moments, leading to the complete definition of the Transfer Matrix Method (TMM).

This method is suitable for in-line systems, where each station is connected by two links to only two other stations, a leading and a following station. The computation starts at the first station, also called left station, it proceeds following the line and ends at the right station. When no automatic computing machines were available, two applications of this approach were very widely used: Holzer's method for torsional vibrations of shafts and Myklestad's method for flexural vibrations of beam-like structures. At the beginning, these methods were adopted for tabular computations, then, with the advent of computers, they were implemented writing strings of code. The main drawback of TMM is that the systems to which it can be applied is limited to inline structures, with neither branches or any multiple connections, making it impossible to write a general code to deal with different geometries. Due to this strong limitation, nowadays this method is no longer in use, because it has been replaced by Finite Element Method (FEM).

The finite element method is used to get a numerical solution, describing the behaviour of a complex system. It consists in meshing the structure, so discretising the model into elements connected by nodes, describing their stiffness and inertia properties with

matrices, reducing the system to a set of ordinary differential equations. The study of finite element method for modelling rotating systems started in 1970, when Ruhl [10] in his PhD dissertation “Dynamics of distributed parameter rotor systems: transfer matrix and finite element techniques” defined an element with the properties of translational inertia and bending stiffness. In 1972, Ruhl and Booker [11] published a more detailed work on this research. Thorkildsen [12] improved this model two years later, including also rotatory inertia and gyroscopic moments. In 1974, Polk [13] published his study on the analysis of natural whirl speeds and critical speeds using a Rayleigh beam finite element; the appendix of the paper contained the first Timoshenko beam finite element, but without any numerical example. In 1976 Nelson and McVaugh [14] published a work with a Rayleigh beam rotating shaft element, similar to Polk’s one and presented the element equations in both fixed and rotating reference frame.

Later in 1977, Zorzi and Nelson [15] made the formulation more general, introducing the expression of internal viscous and hysteretic damping, earlier discussed by Dimaragouas [16] and Gasch [17] in 1976.

In 1980, Nelson [18] presented numerical studies assessing the validity of the elements developed by Polk.

The discretization of a structure is of a great importance in the solution of practical problems because it directly affects the accuracy of the results, in other words, how much it is possible to rely on the model that approximate the real system.

The size of the discrete model should be large enough to give a good representation of the structure, so it is common to have systems of hundreds or even thousands of degrees of freedom. This was a problem before the advent of computers, because only small order matrices could be elaborated. Many methods were developed to reduce to the minimum of size the eigenproblem, or to transform it in an expression that could be solved with particular algorithms.

Nowadays, with the great computational power available, all those techniques are used and this is one of the reason why the FE method has gained so much importance. Once discretised the rotating structure with finite elements, the analysis of its behaviour is related to the resolution of a system of second order ordinary differential equations.

In 1947 Duncan published the work “Mechanical admittances and their applications to oscillation problems” [19], where a procedure to reduce the order of a system of differential equations related to a non rotating structure is presented. In 1957, Frazer, Duncan and Collar dealt with the eigenvalue problem for spinning system, presenting the gyroscopic problem [20]. Later in 1966, Lancaster stated the imaginary conjugate nature of the eigenvalues of an undamped gyroscopic system [21], while Meirovitch and Nelson tackled a damped gyroscopic eigenvalue problem, still solving it numerically [22]. Finally, Meirovitch in 1974 presented a systematic procedure to find eigenvalues and eigenvectors of a complete rotating structure, by reducing the system of n second order ordinary differential equations in a system of $2n$ first order ordinary differential equations [23].

This method is a systematic procedure to solve the eigenproblem and it shows to be computationally very efficient. Nevertheless it has not gained so much popularity with respect to Duncan formulation, so nowadays it is rarely used in computer codes.

1.2 Stability of a rotating structure

The system of second order differential equations can be simplified, obtaining one of first order differential equations with double dimension, to be solved with a modern software. The purpose of the resolution of the set of equations is to find the eigenvalues and eigenvectors of the system, fundamental information to predict the behaviour of the structure at different rotating speeds. Eigenvalues represent the natural frequencies of the rotating system, they depend on the spin speed and their evolution gives the possibility to determine if there are any critical speeds or field of instability. Eigenvectors, or modal shapes, are the mathematical expression of the physical motion of the rotor. It is worth to underline that critical speed and instability threshold are physically different. The first is the spin speed at which the orbit of the rotor is maximum, while the second, if it exists, is the speed at which the orbit starts growing exponentially leading to the failure of the structure. The particular case in which the two numerical values are coincident takes place only for undamped rotating systems, theoretical situation that has no match in reality.

As previously stated, the rotor orbit is related to the spin speed through the natural frequencies, the function describing its evolution in time is reported in Eq. 1.2.1:

$$\delta(t) = \delta_0 e^{St} \quad (1.2.1)$$

where:

- δ_0 is the initial radius of the orbit;
- $S = \text{Re}(S) + i \text{Im}(S)$ is the complex eigenvalue describing the system.

The imaginary part of the solution is the *whirl frequency*, which gives an information on the direction of whirling of the rotor with respect to spinning. Backward whirling motions take place for negative whirling speed, while forward whirling motions correspond to positive whirling speed.

The real part of the solution is the *decay rate*, which gives an information on the modulus of the orbit of the rotor. This is the main parameter to assess the stability: for negative values the orbit slowly decreases, while for positive values of the decay rate the orbit grows exponentially. This will result in strong excitation of the structure and could lead to its failure therefore, to avoid this, stability studies have always to be performed before setting the rotor in operation.

In particular, Lancaster synthesises the concept of stability in [24] stating that a rotating system is:

- *stable* if all eigenvalues are in the open left half of the complex plane. This condition is also referred to as *strong stability*;
- *weakly stable* if all the eigenvalues are in the closed left half of the complex plane and there is at least one pure imaginary eigenvalue. The term *marginal stability* refers to the extreme case of weak stability in which *all* eigenvalues are pure imaginary;
- *unstable* if it is neither stable nor weakly stable, so that there is at least one eigenvalue which is either in the open right half-plane, or is pure imaginary.

A useful way to visualise the analytical study related to stability is the so called Campbell diagram, which takes its name from Wilfred Campbell, English engineer, who first

proposed this graph.

It is a plot of real and imaginary part of the eigenvalues of the system versus the rotor spin speed. Since for a rotating structure the eigenvalues are complex and conjugate, very often the graph reporting the imaginary part is reduced to the first quadrant. This is done by plotting the absolute value of the imaginary part versus the rotating speed and does not lead to any loss of information. Two examples of Campbell diagram are reported in Figure 1.2.1:

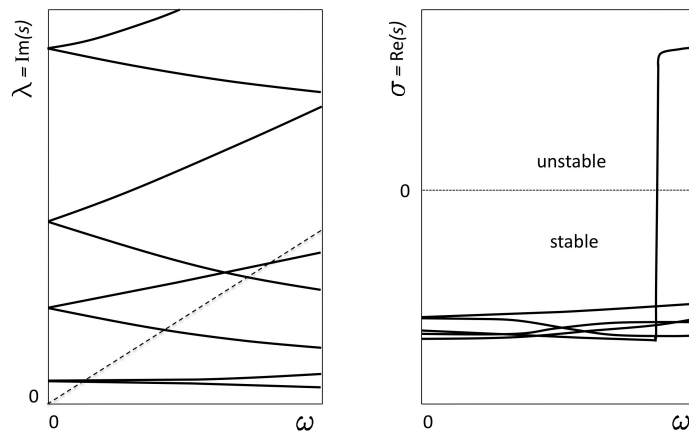


Figure 1.2.1: Forward and backward modes (left) and stability of a rotor (right) [25].

1.3 Stability of a magnetic structure

The stability of a magnetic rotor is not only related to the rotational dynamics, but also to the behaviour of magnetic supports. In this case study, passive magnetic bearings are used to keep the shaft in the correct rotating position. In the field of rotordynamics, they have several advantages with respect to common rolling bearings. First, levitation results in the absence of lubricant, which is a source of friction, and this reflects in no mechanical wear. This is a big issue in systems with traditional supports, because they require constant maintenance in order to avoid damage of the structure. On the contrary, the main issue of magnetic bearings is the need to be located in the right position on the assembly, to maintain the stability conditions on the directions of action.

These devices, which will be later discussed in Sec. (3.1.2), are regulated by the laws

of electromagnetism. The forces exerted on the rotor due to magnetism can be seen as actions of elastic nature, so a linearized model is used and three stiffness can be defined, one for each direction in space. These properties are dependent on the magnetic force and inversely proportional to the distance between the rings, as expressed in Eq. (1.3.1), Eq. (1.3.2) and Eq. (1.3.3).

$$k_{xx} = -\frac{dF_x}{dx} \quad (1.3.1)$$

$$k_{yy} = -\frac{dF_y}{dy} \quad (1.3.2)$$

$$k_{zz} = -\frac{dF_z}{dz} \quad (1.3.3)$$

The elasticity constants have an important role on the stability of the system. This study can be developed referring to Earnshaw's theorem [26], which gives important relations on the magnetic induction vector \mathbf{B} reported in Eq. (1.3.4) and (1.3.5):

$$\nabla^2 \mathbf{B} = 0 \quad (1.3.4)$$

$$\frac{\partial^2 B_x}{\partial x^2} + \frac{\partial^2 B_y}{\partial y^2} + \frac{\partial^2 B_z}{\partial z^2} = 0 \quad (1.3.5)$$

From this formulation it is possible to derive the relation of Eq.(1.3.6) among the magnetic stiffness in the three directions:

$$k_{xx} + k_{yy} + k_{zz} = 0 \quad (1.3.6)$$

Consequently, at least the stiffness on one direction should be positive and it is possible to demonstrate that the condition for the stability holds for negative elastic constant. Therefore, the instability range could be identified with the vertical axis, where a positive stiffness is present, while the other directions are stable holding negative elastic constants.

The magnetic rotor is set to be radially stable and axially unstable.

Chapter 2

Finite element model

A system can be analysed using FEM starting with its discretisation. The structure is subdivided in a series of rod elements, cylindrical objects with inertia and stiffness properties and with negligible internal damping. Springs and dampers of the structure can be modelled with a lumped parameters approach. Spring can be accounted as an elastic element, positioned between two nodes acting on the specified degrees of freedom. Similarly, a damper can be modelled as a damping element, positioned between two nodes acting on the specified degrees of freedom. For both of them, the application point has to be identified with a node and the direction of action has to be specified to link the correct degrees of freedom. Moreover, elasticity and damping constant have to be defined according to the phenomena that are generating them.

Once discretised the structure, the consecutive elements have to be connected and the proper constraints have to be applied. In the case of a rigid structure, the links should be defined in order to reduce the model to a six degrees of freedom system.

2.1 Rod element

The rod element, shown in Figure 2.1.1, is a circular or elliptical pipe located in a reference frame and its axis of rotation coincide with the *x-axis*.

According to the tutorial of the software used for the numerical simulations [27], it is defined as an object between two nodes, where each node is a geometrical point de-

scribed by a 1×4 vector containing the node identification and the three translational coordinates x , y , z .

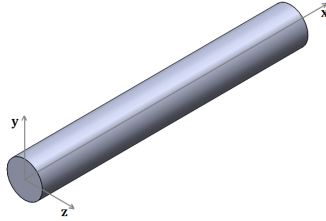


Figure 2.1.1: Rod in a local reference frame

Each node is characterised by six degrees of freedom, reported in Table (2.1.1), consequently the rod behaviour in space is described by twelve degrees of freedom, referred to two nodes.

Generalized DOF	Behaviour
x	<i>axial</i>
y	<i>transversal</i>
z	<i>transversal</i>
r_x	<i>torsional</i>
r_y	<i>flexural</i>
r_z	<i>flexural</i>

Table 2.1.1: Generalized DOF and behaviour

The cross-section of the element can be solid or annular:

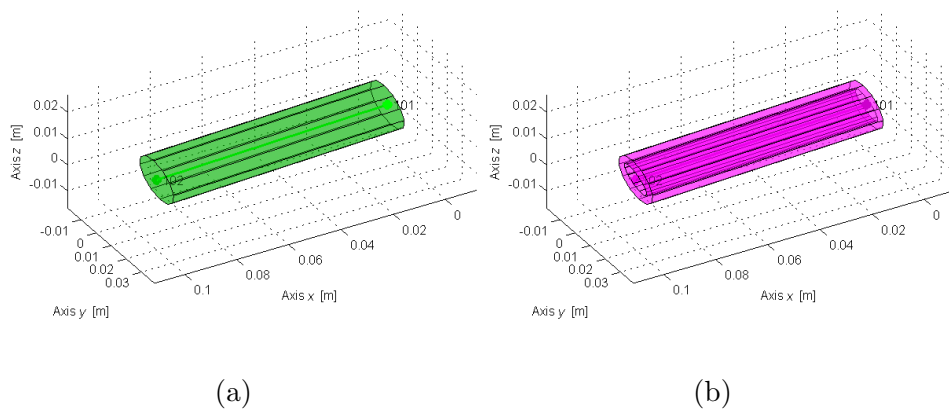


Figure 2.1.2: Rods with solid (a) and annular (b) cross-section [27].

In order to describe completely the rod element, all the information about its properties have to be defined:

- Starting node and ending node of connection of the rod;
- Diameters of the cross-section in y and z directions, to account for circular or elliptical cross-sections;
- Thickness of the rod cross-section for annular cases;
- Density of the rod constitutive material;
- Young modulus of the rod constitutive material;
- Poisson ratio of the rod constitutive material;
- Normal preload on the rod, traction if positive, compression if negative, that produces the pre-stressed stiffness matrix.

Once defined the geometry and the material properties, the dynamic behaviour of a rotating rod with negligible internal damping is described by Eq. 2.1.1:

$$\mathbf{M}_r \ddot{\mathbf{x}} + \Omega \mathbf{G}_r \dot{\mathbf{x}} + (\mathbf{K}_r + \Delta \mathbf{K}_r) \mathbf{x} = \mathbf{f}(t) \quad (2.1.1)$$

where:

- \mathbf{M}_r , \mathbf{K}_r , $\Delta \mathbf{K}_r$ are real 12×12 symmetric matrices describing inertia, stiffness and internal stress properties;
- \mathbf{G}_r is a real 12×12 skew-symmetric matrix describing gyroscopic properties;
- Ω is a scalar representing the rotational speed;
- \mathbf{x} is a 12×1 vector containing the real coordinates of the nodes.

The geometry has an important role in the determination of rod elementary matrices because it affects the behaviour of the structure under stress.

Beam theory states that an elastic object can be defined beam if it has a dimension that is much longer than the other two, but this does not explain the different evolutions of

a slender and a solid beam.

The easiest approach is the so called Euler-Bernoulli theory, which assumes the shear deformation and rotational inertia of the cross section of the rod to be negligible with respect to bending deformation and translational inertia. The derived formulation is suitable to describe slender beam. A structure in which two dimensions become comparable can still be analysed with the beam theory, but the shear deformation and rotational inertia cannot be neglected anymore. A Timoshenko approach accounts for these phenomena, so it is more suitable to describe solid beams. The two approaches are developed under different assumptions, to describe the same type of object whose behaviour changes according to geometrical parameters, so it is not correct to state that one method is better than the other. Anyway, the Euler-Bernoulli formulation can be seen as a particular case of the Timoshenko one, where the shear correction factor is set to zero.

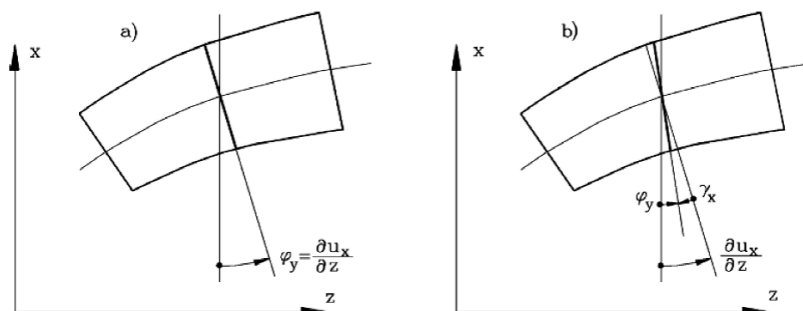


Figure 2.1.3: Effect of shear deformation on bending for Euler Bernoulli beam (a) and Timoshenko beam (b) [1].

Both shear deformation and rotational inertia result in lowering the value of natural frequencies and their effect is increasingly strong with increasing order of the modes. Even if these two approaches are largely used, it has to be underlined that they are formulated under the approximations of the beam theory, so the model is no more suitable when the slenderness becomes too low. Since the beam behaves as solid with increasing order of the modes, high-order modes can be analysed with this theory only if the slenderness is high enough.

2.1.1 Euler-Bernoulli rod element

For an Euler-Bernoulli rod approach, the following coupled mass \mathbf{M}_r , stiffness \mathbf{K}_r , pre-stressed stiffness $\Delta\mathbf{K}_r$ and gyroscopic matrices \mathbf{G}_r are taken into account in a Local Coordinate System (LCS):

$$\mathbf{M}_r = \frac{\rho_r l_r}{420} \begin{bmatrix} 140A_r & 0 & 0 & 0 & 0 & 0 & 70A_r & 0 & 0 & 0 & 0 & 0 \\ 0 & 156A_r & 0 & 0 & 0 & 22l_r A_r & 0 & 54A_r & 0 & 0 & 0 & -13l_r A_r \\ 0 & 0 & 156A_r & 0 & -22l_r A_r & 0 & 0 & 0 & 54A_r & 0 & 13l_r A_r & 0 \\ 0 & 0 & 0 & 140I_{r,O} & 0 & 0 & 0 & 0 & 0 & 70I_{r,O} & 0 & 0 \\ 0 & 0 & -22l_r A_r & 0 & 4l_r^2 A_r & 0 & 0 & 0 & -13l_r A_r & 0 & -3l_r^2 A_r & 0 \\ 0 & 22l_r A_r & 0 & 0 & 0 & 4l_r^2 A_r & 0 & 13l_r A_r & 0 & 0 & 0 & -3l_r^2 A_r \\ 70A_r & 0 & 0 & 0 & 0 & 0 & 140A_r & 0 & 0 & 0 & 0 & 0 \\ 0 & 54A_r & 0 & 0 & 0 & 13l_r A_r & 0 & 156A_r & 0 & 0 & 0 & -22l_r A_r \\ 0 & 0 & 54A_r & 0 & -13l_r A_r & 0 & 0 & 0 & 156A_r & 0 & 22l_r A_r & 0 \\ 0 & 0 & 0 & 70I_{r,O} & 0 & 0 & 0 & 0 & 0 & 140I_{r,O} & 0 & 0 \\ 0 & 0 & 13l_r A_r & 0 & -3l_r^2 A_r & 0 & 0 & 0 & 22l_r A_r & 0 & 4l_r^2 A_r & 0 \\ 0 & -13l_r A_r & 0 & 0 & 0 & -3l_r^2 A_r & 0 & -22l_r A_r & 0 & 0 & 0 & 4l_r^2 A_r \end{bmatrix} \quad (2.1.1.1)$$

$$\mathbf{K}_r = \begin{bmatrix} \frac{E_r A_r}{l_r} & 0 & 0 & 0 & 0 & 0 & -\frac{E_r A_r}{l_r} & 0 & 0 & 0 & 0 & 0 \\ 0 & 12\frac{E_r I_{r,z}}{l_r^3} & 0 & 0 & 0 & 6\frac{E_r I_{r,z}}{l_r^2} & 0 & -12\frac{E_r I_{r,z}}{l_r^3} & 0 & 0 & 0 & 6\frac{E_r I_{r,z}}{l_r^2} \\ 0 & 0 & 12\frac{E_r I_{r,y}}{l_r^3} & 0 & -6\frac{E_r I_{r,y}}{l_r^2} & 0 & 0 & 0 & -12\frac{E_r I_{r,y}}{l_r^3} & 0 & -6\frac{E_r I_{r,y}}{l_r^2} & 0 \\ 0 & 0 & 0 & \frac{G_r J_r}{l_r} & 0 & 0 & 0 & 0 & 0 & -\frac{G_r J_r}{l_r} & 0 & 0 \\ 0 & 0 & -6\frac{E_r I_{r,y}}{l_r^2} & 0 & 4\frac{E_r I_{r,y}}{l_r} & 0 & 0 & 0 & 6\frac{E_r I_{r,y}}{l_r^2} & 0 & 2\frac{E_r I_{r,y}}{l_r} & 0 \\ 0 & 6\frac{E_r I_{r,z}}{l_r^2} & 0 & 0 & 0 & 4\frac{E_r I_{r,z}}{l_r} & 0 & -6\frac{E_r I_{r,z}}{l_r^2} & 0 & 0 & 0 & 2\frac{E_r I_{r,z}}{l_r} \\ -\frac{E_r A_r}{l_r} & 0 & 0 & 0 & 0 & 0 & \frac{E_r A_r}{l_r} & 0 & 0 & 0 & 0 & 0 \\ 0 & -12\frac{E_r I_{r,z}}{l_r^3} & 0 & 0 & 0 & -6\frac{E_r I_{r,z}}{l_r^2} & 0 & 12\frac{E_r I_{r,z}}{l_r^3} & 0 & 0 & 0 & -6\frac{E_r I_{r,z}}{l_r^2} \\ 0 & 0 & -12\frac{E_r I_{r,y}}{l_r^3} & 0 & 6\frac{E_r I_{r,y}}{l_r^2} & 0 & 0 & 0 & 12\frac{E_r I_{r,y}}{l_r^3} & 0 & 6\frac{E_r I_{r,y}}{l_r^2} & 0 \\ 0 & 0 & 0 & -\frac{G_r J_r}{l_r} & 0 & 0 & 0 & 0 & 0 & \frac{G_r J_r}{l_r} & 0 & 0 \\ 0 & 0 & -6\frac{E_r I_{r,y}}{l_r^2} & 0 & 2\frac{E_r I_{r,y}}{l_r} & 0 & 0 & 0 & 6\frac{E_r I_{r,y}}{l_r^2} & 0 & 4\frac{E_r I_{r,y}}{l_r} & 0 \\ 0 & 6\frac{E_r I_{r,z}}{l_r^2} & 0 & 0 & 0 & 2\frac{E_r I_{r,z}}{l_r} & 0 & -6\frac{E_r I_{r,z}}{l_r^2} & 0 & 0 & 0 & 4\frac{E_r I_{r,z}}{l_r} \end{bmatrix} \quad (2.1.1.2)$$

$$\Delta \mathbf{K}_r = \frac{N}{30l_r} \begin{bmatrix} 0 & 0 & 0 & 0 & 0 & 0 & 0 & 0 & 0 & 0 & 0 & 0 \\ 0 & 36 & 0 & 0 & 0 & 3l_r & 0 & -36 & 0 & 0 & 0 & 3l_r \\ 0 & 0 & 36 & 0 & -3l_r & 0 & 0 & 0 & -36 & 0 & -3l_r & 0 \\ 0 & 0 & 0 & 0 & 0 & 0 & 0 & 0 & 0 & 0 & 0 & 0 \\ 0 & 0 & -3l_r & 0 & 4l_r^2 & 0 & 0 & 0 & 3l_r & 0 & -l_r^2 & 0 \\ 0 & 3l_r & 0 & 0 & 0 & 4l_r^2 & 0 & -3l_r & 0 & 0 & 0 & -l_r^2 \\ 0 & 0 & 0 & 0 & 0 & 0 & 0 & 0 & 0 & 0 & 0 & 0 \\ 0 & -36 & 0 & 0 & 0 & -3l_r & 0 & 36 & 0 & 0 & 0 & -3l_r \\ 0 & 0 & -36 & 0 & 3l_r & 0 & 0 & 0 & 36 & 0 & 3l_r & 0 \\ 0 & 0 & 0 & 0 & 0 & 0 & 0 & 0 & 0 & 0 & 0 & 0 \\ 0 & 0 & -3l_r & 0 & -l_r^2 & 0 & 0 & 0 & 3l_r & 0 & 4l_r^2 & 0 \\ 0 & 3l_r & 0 & 0 & 0 & -l_r^2 & 0 & -3l_r & 0 & 0 & 0 & 4l_r^2 \end{bmatrix} \quad (2.1.1.3)$$

$$\mathbf{G}_r = -\frac{\rho_r}{30l_r} \begin{bmatrix} 0 & 0 & 0 & 0 & 0 & 0 & 0 & 0 & 0 & 0 & 0 & 0 \\ 0 & 0 & -72I_{r,z} & 0 & 6l_r I_{r,z} & 0 & 0 & 0 & 72I_{r,z} & 0 & 6l_r I_{r,z} & 0 \\ 0 & 72I_{r,y} & 0 & 0 & 0 & 6l_r I_{r,y} & 0 & -72I_{r,y} & 0 & 0 & 0 & 6l_r I_{r,y} \\ 0 & 0 & 0 & 0 & 0 & 0 & 0 & 0 & 0 & 0 & 0 & 0 \\ 0 & -6l_r I_{r,y} & 0 & 0 & 0 & -8l_r^2 I_{r,y} & 0 & 6l_r I_{r,y} & 0 & 0 & 0 & 2l_r^2 I_{r,y} \\ 0 & 0 & -6l_r I_{r,z} & 0 & 8l_r^2 I_{r,z} & 0 & 0 & 0 & 6l_r I_{r,z} & 0 & -2l_r^2 I_{r,z} & 0 \\ 0 & 0 & 0 & 0 & 0 & 0 & 0 & 0 & 0 & 0 & 0 & 0 \\ 0 & 0 & 72I_{r,z} & 0 & -6l_r I_{r,z} & 0 & 0 & 0 & -72I_{r,z} & 0 & -6l_r I_{r,z} & 0 \\ 0 & -72I_{r,y} & 0 & 0 & 0 & -6l_r I_{r,y} & 0 & 72I_{r,y} & 0 & 0 & 0 & -6l_r I_{r,y} \\ 0 & 0 & 0 & 0 & 0 & 0 & 0 & 0 & 0 & 0 & 0 & 0 \\ 0 & -6l_r I_{r,y} & 0 & 0 & 0 & 2l_r^2 I_{r,y} & 0 & 6l_r I_{r,y} & 0 & 0 & 0 & -8l_r^2 I_{r,y} \\ 0 & 0 & -6l_r I_{r,z} & 0 & -2l_r^2 I_{r,z} & 0 & 0 & 0 & 6l_r I_{r,z} & 0 & 8l_r^2 I_{r,z} & 0 \end{bmatrix} \quad (2.1.1.4)$$

where the following rod (r) geometrical properties are:

- ρ_r , E_r , G_r are rod material properties and respectively density [kg/m^3], Young modulus [Pa] and tangential modulus [Pa];
- l_r is the rod length [m];
- D_y , D_z , t are respectively the diameters along rod local y and z directions and the rod thickness [m]; it is worth noting that $0 < 2t \leq \min(D_y, D_z)$;

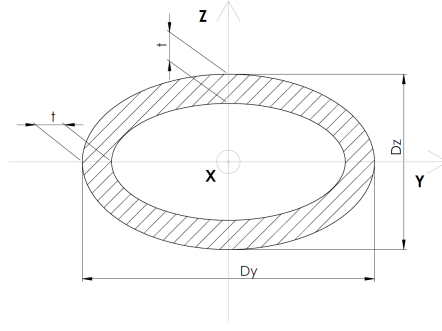


Figure 2.1.1.1: Rod cross-section parameters [27].

- $A_r = A_{r,ex} - A_{r,in} = \frac{\pi}{4} [Dy Dz - (Dy - 2t) (Dz - 2t)]$ is the cross-section area [m^2] computed as the difference between external and inner area;
- $I_{r,y} = \frac{\pi}{64} [Dy Dz^3 - (Dy - 2t) (Dz - 2t)^3], I_{r,z} = \frac{\pi}{64} [Dy^3 Dz - (Dy - 2t)^3 (Dz - 2t)]$ are the second moments of area with respect to cross-section axes y or z [m^4];
- $I_{r,O} = I_{r,y} + I_{r,z} = \frac{1}{16} \{ (Dy^2 + Dz^2) A_{r,ex} - [(Dy - 2t)^2 + (Dz - 2t)^2] A_{r,in} \}$ is the polar moment of area of the cross-section [m^4];
- both for circular or elliptical, solid or annular cross-section, the torsional polar moment of area [m^4] is evaluated through the expression:

$$J_r = \frac{\pi}{16} (1 - m^4) \frac{Dy^3 Dz^3}{Dy^2 + Dz^2} = \frac{\pi}{16} \psi_r Dy Dz^3 \quad (2.1.1.5)$$

where $0 \leq m = 1 - \frac{2t}{\min(Dy, Dz)} < 1$ and in the following $Dy \geq Dz$ is assumed. The coefficient for the torsional behaviour results $\psi_r = \frac{1-m^4}{1+(\frac{Dz}{Dy})^2}$ is valid especially also to thick-walled annular cross-section.

2.1.2 Timoshenko rod element

For a Timoshenko rod approach, the following coupled mass \mathbf{M}_r , stiffness \mathbf{K}_r , pre-stressed stiffness $\Delta\mathbf{K}_r$ and gyroscopic matrices \mathbf{G}_r are taken into account in a Local Coordinate System (LCS):

$$\mathbf{M}_r = \frac{\rho_r l_r}{420} \begin{bmatrix} 140A_r & 0 & 0 & 0 & 0 & 0 & 70A_r & 0 & 0 & 0 & 0 & 0 \\ 0 & \frac{m_{1,y} A_r}{(1+\Phi_y)^2} & 0 & 0 & 0 & \frac{m_{2,y} l_r A_r}{(1+\Phi_y)^2} & 0 & \frac{m_{3,y} A_r}{(1+\Phi_y)^2} & 0 & 0 & 0 & -\frac{m_{4,y} l_r A_r}{(1+\Phi_y)^2} \\ 0 & 0 & \frac{m_{1,z} A_r}{(1+\Phi_z)^2} & 0 & -\frac{m_{2,z} l_r A_r}{(1+\Phi_z)^2} & 0 & 0 & 0 & \frac{m_{3,z} A_r}{(1+\Phi_z)^2} & 0 & \frac{m_{4,z} l_r A_r}{(1+\Phi_z)^2} & 0 \\ 0 & 0 & 0 & 140I_{r,O} & 0 & 0 & 0 & 0 & 0 & 70I_{r,O} & 0 & 0 \\ 0 & 0 & -\frac{m_{2,z} l_r A_r}{(1+\Phi_z)^2} & 0 & \frac{m_{5,z} l_r^2 A_r}{(1+\Phi_z)^2} & 0 & 0 & 0 & -\frac{m_{4,z} l_r A_r}{(1+\Phi_z)^2} & 0 & -\frac{m_{6,z} l_r^2 A_r}{(1+\Phi_z)^2} & 0 \\ 0 & \frac{m_{2,y} l_r A_r}{(1+\Phi_y)^2} & 0 & 0 & 0 & \frac{m_{5,y} l_r^2 A_r}{(1+\Phi_y)^2} & 0 & \frac{m_{4,y} l_r A_r}{(1+\Phi_y)^2} & 0 & 0 & 0 & -\frac{m_{6,y} l_r^2 A_r}{(1+\Phi_y)^2} \\ 70A_r & 0 & 0 & 0 & 0 & 0 & 140A_r & 0 & 0 & 0 & 0 & 0 \\ 0 & \frac{m_{3,y} A_r}{(1+\Phi_y)^2} & 0 & 0 & 0 & \frac{m_{4,y} l_r A_r}{(1+\Phi_y)^2} & 0 & \frac{m_{1,y} A_r}{(1+\Phi_y)^2} & 0 & 0 & 0 & -\frac{m_{2,y} l_r A_r}{(1+\Phi_y)^2} \\ 0 & 0 & \frac{m_{3,z} A_r}{(1+\Phi_z)^2} & 0 & -\frac{m_{4,z} l_r A_r}{(1+\Phi_z)^2} & 0 & 0 & 0 & \frac{m_{1,z} A_r}{(1+\Phi_z)^2} & 0 & \frac{m_{2,z} l_r A_r}{(1+\Phi_z)^2} & 0 \\ 0 & 0 & 0 & 70I_{r,O} & 0 & 0 & 0 & 0 & 0 & 140I_{r,O} & 0 & 0 \\ 0 & 0 & \frac{m_{4,z} l_r A_r}{(1+\Phi_z)^2} & 0 & -\frac{m_{6,z} l_r^2 A_r}{(1+\Phi_z)^2} & 0 & 0 & 0 & \frac{m_{2,z} l_r A_r}{(1+\Phi_z)^2} & 0 & \frac{m_{5,z} l_r^2 A_r}{(1+\Phi_z)^2} & 0 \\ 0 & -\frac{m_{4,y} l_r A_r}{(1+\Phi_y)^2} & 0 & 0 & 0 & -\frac{m_{6,y} l_r^2 A_r}{(1+\Phi_y)^2} & 0 & -\frac{m_{2,y} l_r A_r}{(1+\Phi_y)^2} & 0 & 0 & 0 & \frac{m_{5,y} l_r^2 A_r}{(1+\Phi_y)^2} \end{bmatrix} +$$

$$+ \frac{\rho_r}{30I_r} \begin{bmatrix} 0 & 0 & 0 & 0 & 0 & 0 & 0 & 0 & 0 & 0 & 0 & 0 \\ 0 & \frac{m_{7,y} l_r I_{r,z}}{(1+\Phi_y)^2} & 0 & 0 & 0 & \frac{m_{8,y} l_r I_{r,z}}{(1+\Phi_y)^2} & 0 & -\frac{m_{7,y} I_{r,z}}{(1+\Phi_y)^2} & 0 & 0 & 0 & \frac{m_{8,y} l_r I_{r,z}}{(1+\Phi_y)^2} \\ 0 & 0 & \frac{m_{7,z} l_r I_{r,y}}{(1+\Phi_z)^2} & 0 & -\frac{m_{8,z} l_r I_{r,y}}{(1+\Phi_z)^2} & 0 & 0 & 0 & -\frac{m_{7,z} l_r I_{r,y}}{(1+\Phi_z)^2} & 0 & -\frac{m_{7,z} l_r I_{r,y}}{(1+\Phi_z)^2} & 0 \\ 0 & 0 & 0 & 0 & 0 & 0 & 0 & 0 & 0 & 0 & 0 & 0 \\ 0 & 0 & -\frac{m_{8,z} l_r I_{r,y}}{(1+\Phi_z)^2} & 0 & \frac{m_{9,z} l_r^2 I_{r,y}}{(1+\Phi_z)^2} & 0 & 0 & 0 & \frac{m_{8,z} l_r I_{r,y}}{(1+\Phi_z)^2} & 0 & -\frac{m_{10,z} l_r^2 I_{r,y}}{(1+\Phi_z)^2} & 0 \\ 0 & \frac{m_{8,y} l_r I_{r,z}}{(1+\Phi_y)^2} & 0 & 0 & 0 & \frac{m_{9,y} l_r^2 I_{r,z}}{(1+\Phi_y)^2} & 0 & -\frac{m_{8,y} l_r I_{r,z}}{(1+\Phi_y)^2} & 0 & 0 & 0 & -\frac{m_{10,y} l_r^2 I_{r,z}}{(1+\Phi_y)^2} \\ 0 & 0 & 0 & 0 & 0 & 0 & 0 & 0 & 0 & 0 & 0 & 0 \\ 0 & -\frac{m_{7,y} l_r I_{r,z}}{(1+\Phi_y)^2} & 0 & 0 & 0 & -\frac{m_{8,y} l_r I_{r,z}}{(1+\Phi_y)^2} & 0 & \frac{m_{7,y} l_r I_{r,z}}{(1+\Phi_y)^2} & 0 & 0 & 0 & -\frac{m_{8,y} l_r I_{r,z}}{(1+\Phi_y)^2} \\ 0 & 0 & -\frac{m_{7,z} l_r I_{r,y}}{(1+\Phi_z)^2} & 0 & \frac{m_{8,z} l_r I_{r,y}}{(1+\Phi_z)^2} & 0 & 0 & 0 & \frac{m_{7,z} l_r I_{r,y}}{(1+\Phi_z)^2} & 0 & \frac{m_{8,z} l_r I_{r,y}}{(1+\Phi_z)^2} & 0 \\ 0 & 0 & 0 & 0 & 0 & 0 & 0 & 0 & 0 & 0 & 0 & 0 \\ 0 & 0 & -\frac{m_{8,z} l_r I_{r,y}}{(1+\Phi_z)^2} & 0 & \frac{m_{10,z} l_r^2 I_{r,y}}{(1+\Phi_z)^2} & 0 & 0 & 0 & \frac{m_{8,z} l_r I_{r,y}}{(1+\Phi_z)^2} & 0 & \frac{m_{9,z} l_r^2 I_{r,y}}{(1+\Phi_z)^2} & 0 \\ 0 & \frac{m_{8,y} l_r I_{r,z}}{(1+\Phi_y)^2} & 0 & 0 & 0 & -\frac{m_{10,y} l_r^2 I_{r,z}}{(1+\Phi_y)^2} & 0 & -\frac{m_{8,y} l_r I_{r,z}}{(1+\Phi_y)^2} & 0 & 0 & 0 & \frac{m_{9,y} l_r^2 I_{r,z}}{(1+\Phi_y)^2} \end{bmatrix} \quad (2.1.2.1)$$

$$\mathbf{K}_r = \begin{bmatrix} \frac{E_r A_r}{l_r} & 0 & 0 & 0 & 0 & 0 & -\frac{E_r A_r}{l_r} & 0 & 0 & 0 & 0 & 0 \\ 0 & 12 \frac{E_r I_{r,z}}{l_r^3 (1+\Phi_y)} & 0 & 0 & 0 & 0 & 6 \frac{E_r I_{r,z}}{l_r^2 (1+\Phi_y)} & 0 & -12 \frac{E_r I_{r,z}}{l_r^3 (1+\Phi_y)} & 0 & 0 & 0 & 6 \frac{E_r I_{r,z}}{l_r^2 (1+\Phi_y)} \\ 0 & 0 & 12 \frac{E_r I_{r,y}}{l_r^3 (1+\Phi_z)} & 0 & -6 \frac{E_r I_{r,y}}{l_r^2 (1+\Phi_z)} & 0 & 0 & 0 & -12 \frac{E_r I_{r,y}}{l_r^3 (1+\Phi_z)} & 0 & -6 \frac{E_r I_{r,y}}{l_r^2 (1+\Phi_z)} & 0 \\ 0 & 0 & 0 & \frac{G_r J_r}{l_r} & 0 & 0 & 0 & 0 & 0 & 0 & -\frac{G_r J_r}{l_r} & 0 & 0 \\ 0 & 0 & -6 \frac{E_r I_{r,y}}{l_r^2 (1+\Phi_z)} & 0 & \frac{E_r I_{r,y}}{l_r} \frac{4+\Phi_z}{1+\Phi_z} & 0 & 0 & 0 & 6 \frac{E_r I_{r,y}}{l_r^2 (1+\Phi_z)} & 0 & \frac{E_r I_{r,y}}{l_r} \frac{2-\Phi_z}{1+\Phi_z} & 0 & 0 \\ 0 & 6 \frac{E_r I_{r,z}}{l_r^2 (1+\Phi_y)} & 0 & 0 & 0 & \frac{E_r I_{r,z}}{l_r} \frac{4+\Phi_y}{1+\Phi_y} & 0 & -6 \frac{E_r I_{r,z}}{l_r^2 (1+\Phi_y)} & 0 & 0 & 0 & \frac{E_r I_{r,z}}{l_r} \frac{2-\Phi_y}{1+\Phi_y} & 0 \\ -\frac{E_r A_r}{l_r} & 0 & 0 & 0 & 0 & 0 & \frac{E_r A_r}{l_r} & 0 & 0 & 0 & 0 & 0 & 0 \\ 0 & -12 \frac{E_r I_{r,z}}{l_r^3 (1+\Phi_y)} & 0 & 0 & 0 & 0 & -6 \frac{E_r I_{r,z}}{l_r^2 (1+\Phi_y)} & 0 & 12 \frac{E_r I_{r,z}}{l_r^3 (1+\Phi_y)} & 0 & 0 & 0 & -6 \frac{E_r I_{r,z}}{l_r^2 (1+\Phi_y)} \\ 0 & 0 & -12 \frac{E_r I_{r,y}}{l_r^3 (1+\Phi_z)} & 0 & 6 \frac{E_r I_{r,y}}{l_r^2 (1+\Phi_z)} & 0 & 0 & 0 & -12 \frac{E_r I_{r,y}}{l_r^3 (1+\Phi_z)} & 0 & 6 \frac{E_r I_{r,y}}{l_r^2 (1+\Phi_z)} & 0 & 0 \\ 0 & 0 & 0 & -\frac{G_r J_r}{l_r} & 0 & 0 & 0 & 0 & 0 & 0 & \frac{G_r J_r}{l_r} & 0 & 0 \\ 0 & 0 & -6 \frac{E_r I_{r,y}}{l_r^2 (1+\Phi_z)} & 0 & \frac{E_r I_{r,y}}{l_r} \frac{2-\Phi_z}{1+\Phi_z} & 0 & 0 & 0 & 6 \frac{E_r I_{r,y}}{l_r^2 (1+\Phi_z)} & 0 & \frac{E_r I_{r,y}}{l_r} \frac{4+\Phi_z}{1+\Phi_z} & 0 & 0 \\ 0 & 6 \frac{E_r I_{r,z}}{l_r^2 (1+\Phi_y)} & 0 & 0 & 0 & \frac{E_r I_{r,z}}{l_r} \frac{2-\Phi_y}{1+\Phi_y} & 0 & -6 \frac{E_r I_{r,z}}{l_r^2 (1+\Phi_y)} & 0 & 0 & 0 & \frac{E_r I_{r,z}}{l_r} \frac{4+\Phi_y}{1+\Phi_y} & 0 \end{bmatrix} \quad (2.1.2.2)$$

$$\mathbf{G}_r = \mathbf{G}_0 + \mathbf{G}_\Phi + \mathbf{G}_{\Phi^2} \quad (2.1.2.7)$$

where:

$$\mathbf{G}_0 = -\frac{\rho_r}{30l_r} \begin{bmatrix} 0 & 0 & 0 & 0 & 0 & 0 & 0 & 0 & 0 & 0 & 0 & 0 \\ 0 & 0 & -\frac{72I_{r,z}}{(1+\Phi_y)^2} & \frac{6I_r I_{r,z}}{(1+\Phi_y)^2} & 0 & 0 & 0 & \frac{72I_r I_{r,z}}{(1+\Phi_y)^2} & \frac{6I_r I_{r,z}}{(1+\Phi_y)^2} & 0 & 0 \\ 0 & \frac{72I_{r,y}}{(1+\Phi_z)^2} & 0 & 0 & 0 & \frac{6I_r I_{r,y}}{(1+\Phi_z)^2} & 0 & -\frac{72I_{r,y}}{(1+\Phi_z)^2} & 0 & 0 & 0 & \frac{6I_r I_{r,y}}{(1+\Phi_z)^2} \\ 0 & 0 & 0 & 0 & 0 & 0 & 0 & 0 & 0 & 0 & 0 & 0 \\ 0 & -\frac{6I_r I_{r,y}}{(1+\Phi_z)^2} & 0 & 0 & 0 & -\frac{8I_r^2 I_{r,y}}{(1+\Phi_z)^2} & 0 & \frac{6I_r I_{r,y}}{(1+\Phi_z)^2} & 0 & 0 & 0 & \frac{2I_r^2 I_{r,y}}{(1+\Phi_z)^2} \\ 0 & 0 & -\frac{6I_r I_{r,z}}{(1+\Phi_y)^2} & \frac{8I_r^2 I_{r,z}}{(1+\Phi_y)^2} & 0 & 0 & 0 & \frac{6I_r I_{r,z}}{(1+\Phi_y)^2} & 0 & -\frac{2I_r^2 I_{r,z}}{(1+\Phi_y)^2} & 0 & 0 \\ 0 & 0 & 0 & 0 & 0 & 0 & 0 & 0 & 0 & 0 & 0 & 0 \\ 0 & 0 & \frac{72I_{r,z}}{(1+\Phi_y)^2} & -\frac{6I_r I_{r,z}}{(1+\Phi_y)^2} & 0 & 0 & 0 & -\frac{72I_{r,z}}{(1+\Phi_y)^2} & 0 & -\frac{6I_r I_{r,z}}{(1+\Phi_y)^2} & 0 & 0 \\ 0 & -\frac{72I_{r,y}}{(1+\Phi_z)^2} & 0 & 0 & 0 & -\frac{6I_r I_{r,y}}{(1+\Phi_z)^2} & 0 & \frac{72I_{r,y}}{(1+\Phi_z)^2} & 0 & 0 & 0 & -\frac{6I_r I_{r,y}}{(1+\Phi_z)^2} \\ 0 & 0 & 0 & 0 & 0 & 0 & 0 & 0 & 0 & 0 & 0 & 0 \\ 0 & -\frac{6I_r I_{r,y}}{(1+\Phi_z)^2} & 0 & 0 & 0 & \frac{2I_r^2 I_{r,y}}{(1+\Phi_z)^2} & 0 & \frac{6I_r I_{r,y}}{(1+\Phi_z)^2} & 0 & 0 & 0 & -\frac{8I_r^2 I_{r,y}}{(1+\Phi_z)^2} \\ 0 & 0 & -\frac{6I_r I_{r,z}}{(1+\Phi_y)^2} & -\frac{2I_r^2 I_{r,z}}{(1+\Phi_y)^2} & 0 & 0 & 0 & \frac{6I_r I_{r,z}}{(1+\Phi_y)^2} & 0 & \frac{8I_r^2 I_{r,z}}{(1+\Phi_y)^2} & 0 & 0 \end{bmatrix} \quad (2.1.2.8)$$

$$\mathbf{G}_\Phi = -\frac{\rho_r}{30l_r} \begin{bmatrix} 0 & 0 & 0 & 0 & 0 & 0 & 0 & 0 & 0 & 0 & 0 & 0 \\ 0 & 0 & 0 & 0 & -\frac{30I_r I_{r,z}}{(1+\Phi_y)^2} \Phi_y & 0 & 0 & 0 & 0 & 0 & -\frac{30I_r I_{r,z}}{(1+\Phi_y)^2} \Phi_y & 0 \\ 0 & 0 & 0 & 0 & 0 & -\frac{30I_r I_{r,y}}{(1+\Phi_z)^2} \Phi_z & 0 & 0 & 0 & 0 & 0 & -\frac{30I_r I_{r,y}}{(1+\Phi_z)^2} \Phi_z \\ 0 & 0 & 0 & 0 & 0 & 0 & 0 & 0 & 0 & 0 & 0 & 0 \\ 0 & \frac{30I_r I_{r,y}}{(1+\Phi_z)^2} \Phi_z & 0 & 0 & 0 & -\frac{10I_r^2 I_{r,y}}{(1+\Phi_z)^2} \Phi_z & 0 & -\frac{30I_r I_{r,y}}{(1+\Phi_z)^2} \Phi_z & 0 & 0 & 0 & \frac{10I_r^2 I_{r,y}}{(1+\Phi_z)^2} \Phi_z \\ 0 & 0 & \frac{30I_r I_{r,z}}{(1+\Phi_y)^2} \Phi_y & 0 & \frac{10I_r^2 I_{r,z}}{(1+\Phi_y)^2} \Phi_y & 0 & 0 & 0 & -\frac{30I_r I_{r,z}}{(1+\Phi_y)^2} \Phi_y & 0 & -\frac{10I_r^2 I_{r,z}}{(1+\Phi_y)^2} \Phi_y & 0 \\ 0 & 0 & 0 & 0 & 0 & 0 & 0 & 0 & 0 & 0 & 0 & 0 \\ 0 & 0 & 0 & 0 & \frac{30I_r I_{r,z}}{(1+\Phi_y)^2} \Phi_y & 0 & 0 & 0 & 0 & 0 & \frac{30I_r I_{r,z}}{(1+\Phi_y)^2} \Phi_y & 0 \\ 0 & 0 & 0 & 0 & 0 & \frac{30I_r I_{r,y}}{(1+\Phi_z)^2} \Phi_z & 0 & 0 & 0 & 0 & 0 & \frac{30I_r I_{r,y}}{(1+\Phi_z)^2} \Phi_z \\ 0 & 0 & 0 & 0 & 0 & 0 & 0 & 0 & 0 & 0 & 0 & 0 \\ 0 & \frac{30I_r I_{r,y}}{(1+\Phi_z)^2} \Phi_z & 0 & 0 & 0 & \frac{10I_r^2 I_{r,y}}{(1+\Phi_z)^2} \Phi_z & 0 & -\frac{30I_r I_{r,y}}{(1+\Phi_z)^2} \Phi_z & 0 & 0 & 0 & -\frac{10I_r^2 I_{r,y}}{(1+\Phi_z)^2} \Phi_z \\ 0 & 0 & \frac{30I_r I_{r,z}}{(1+\Phi_y)^2} \Phi_y & 0 & -\frac{10I_r^2 I_{r,z}}{(1+\Phi_y)^2} \Phi_y & 0 & 0 & 0 & -\frac{30I_r I_{r,z}}{(1+\Phi_y)^2} \Phi_y & 0 & \frac{10I_r^2 I_{r,z}}{(1+\Phi_y)^2} \Phi_y & 0 \end{bmatrix} \quad (2.1.2.9)$$

$$\mathbf{G}_{\Phi^2} = -\frac{\rho_r}{30l_r} \begin{bmatrix} 0 & 0 & 0 & 0 & 0 & 0 & 0 & 0 & 0 & 0 & 0 \\ 0 & 0 & 0 & 0 & 0 & 0 & 0 & 0 & 0 & 0 & 0 \\ 0 & 0 & 0 & 0 & 0 & 0 & 0 & 0 & 0 & 0 & 0 \\ 0 & 0 & 0 & 0 & 0 & 0 & 0 & 0 & 0 & 0 & 0 \\ 0 & 0 & 0 & 0 & -\frac{20I_r^2 I_{r,y}}{(1+\Phi_z)^2} \Phi_z^2 & 0 & 0 & 0 & 0 & 0 & -\frac{10I_r^2 I_{r,y}}{(1+\Phi_z)^2} \Phi_z^2 \\ 0 & 0 & 0 & \frac{20I_r^2 I_{r,z}}{(1+\Phi_y)^2} \Phi_y^2 & 0 & 0 & 0 & 0 & \frac{10I_r^2 I_{r,z}}{(1+\Phi_y)^2} \Phi_y^2 & 0 & 0 \\ 0 & 0 & 0 & 0 & 0 & 0 & 0 & 0 & 0 & 0 & 0 \\ 0 & 0 & 0 & 0 & 0 & 0 & 0 & 0 & 0 & 0 & 0 \\ 0 & 0 & 0 & 0 & 0 & 0 & 0 & 0 & 0 & 0 & 0 \\ 0 & 0 & 0 & 0 & 0 & 0 & 0 & 0 & 0 & 0 & 0 \\ 0 & 0 & 0 & 0 & -\frac{10I_r^2 I_{r,y}}{(1+\Phi_z)^2} \Phi_z^2 & 0 & 0 & 0 & 0 & 0 & -\frac{20I_r^2 I_{r,y}}{(1+\Phi_z)^2} \Phi_z^2 \\ 0 & 0 & 0 & \frac{10I_r^2 I_{r,z}}{(1+\Phi_y)^2} \Phi_y^2 & 0 & 0 & 0 & 0 & \frac{20I_r^2 I_{r,z}}{(1+\Phi_y)^2} \Phi_y^2 & 0 & 0 \end{bmatrix} \quad (2.1.2.10)$$

The rod (r) geometrical properties are the same of the Euler-Bernoulli formulation and:

- $\Phi_y = \frac{12 E_r I_{r,z}}{A_r G_r k_{r,y} l_r^2}$, $\Phi_z = \frac{12 E_r I_{r,y}}{A_r G_r k_{r,z} l_r^2}$ are the ratios between the shear and the flexural flexibility of the beam in y and z direction;

- all the masses, used in the consistent mass matrix reported in Eq. (2.1.2.1), are the following:

$$m_1 = 156 + 294 \Phi + 140 \Phi^2, \quad m_2 = 22 + 38.5 \Phi + 17.5 \Phi^2, \quad m_3 = 54 + 126 \Phi + 70 \Phi^2,$$

$$\begin{aligned}
 m_4 &= 13 + 31.5 \Phi + 17.5 \Phi^2, & m_5 &= 4 + 7 \Phi + 3.5 \Phi^2, \\
 m_6 &= 3 + 7 \Phi + 3.5 \Phi^2, & m_7 &= 36, & m_8 &= 3 - 15 \Phi, \\
 m_9 &= 4 + 5 \Phi + 10 \Phi^2, & m_{10} &= 1 + 5 \Phi - 5 \Phi^2;
 \end{aligned}$$

- $k_{r,y}, k_{r,z}$ are the shear correction factors in y and z directions;
- for circular or elliptical, solid or annular cross-section, the shear factors $k_{r,y}, k_{r,z}$ are equal to k_r and evaluated through the expression [28]:

$$k_r = \frac{12 (1 + \nu_r) (3 + n^2)}{40 + 37 \nu_r + (16 + 10 \nu_r) n^2 + \nu_r n^4} \frac{5 \pi (1 + m^2)^2}{(1.495 - 0.192 \nu_r + 0.078 \nu_r^2) (3 \pi m^4 + (8 m^3 + 4m) \sqrt{1 - m^2} + 13 \pi m) + 16 m^2 \sin^{-1}(m) - 4 \sin^{-1}(m) + 5 \pi} \quad (2.1.2.11)$$

where:

$$0 \leq m = 1 - \frac{2t}{\min(Dy, Dz)} < 1, 1 \leq n = \frac{\max(Dy, Dz)}{\min(Dy, Dz)} < +\infty$$

2.2 Assembly of the structure

2.2.1 From local to global reference frame

The equations of motions of a rod element are written in a Local Coordinate System. It follows that all the elementary matrices expressed in Sec. (2.1) are referred to a reference frame integral with the cylinder. In order to describe the behaviour of the whole structure, another reference frame is defined, called Global Coordinate System (GCS). The procedure to pass from a local to a global definition of the elementary matrices consists in applying the proper rotations.

For each rod it is possible to define α , a vector containing the rotations of each element around the x -axis of the GCS, β , a vector containing the rotations of each element around the y -axis of the GCS, and γ , a vector containing the rotations of each element around the z -axis of the GCS.

Three independent rotations of angles α, β, γ are performed to locate the rod, aligned to the x -axis, to its end node:

$$\mathbf{R}_{xyz} = \mathbf{R}_x \mathbf{R}_y \mathbf{R}_z = \begin{bmatrix} 1 & 0 & 0 \\ 0 & \cos \alpha & \sin \alpha \\ 0 & \sin \alpha & \cos \alpha \end{bmatrix} \begin{bmatrix} \cos \beta & 0 & -\sin \beta \\ 0 & 1 & 0 \\ \sin \beta & 0 & \cos \beta \end{bmatrix} \begin{bmatrix} \cos \gamma & \sin \gamma & 0 \\ -\sin \gamma & \cos \gamma & 0 \\ 0 & 0 & 1 \end{bmatrix} \quad (2.2.1.1)$$

$$\mathbf{T}_{xyz} = \begin{bmatrix} \mathbf{R}_{xyz} & 0 & 0 & 0 \\ 0 & \mathbf{R}_{xyz} & 0 & 0 \\ 0 & 0 & \mathbf{R}_{xyz} & 0 \\ 0 & 0 & 0 & \mathbf{R}_{xyz} \end{bmatrix} \quad (2.2.1.2)$$

By applying the transformation matrix to the elementary matrices, it is possible to find their expressions in the global coordinate system:

$$\mathbf{M}_{r,GCS} = \mathbf{T}_{xyz}^T \mathbf{M}_r \mathbf{T}_{xyz} \quad (2.2.1.3)$$

$$\mathbf{G}_{r,GCS} = \mathbf{T}_{xyz}^T \mathbf{G}_r \mathbf{T}_{xyz} \quad (2.2.1.4)$$

$$\mathbf{C}_{r,GCS} = \mathbf{T}_{xyz}^T \mathbf{C}_r \mathbf{T}_{xyz} \quad (2.2.1.5)$$

$$\mathbf{K}_{r,GCS} = \mathbf{T}_{xyz}^T (\mathbf{K}_r + \Delta \mathbf{K}_r) \mathbf{T}_{xyz} \quad (2.2.1.6)$$

The operation to pass from local to global coordinates is a composition of rotations, therefore the values contained inside the matrices are not changed but just moved in another position. It is evident that having neglected the internal damping of the rod results in having a zeros matrix in the GCS, as it was in the LCS.

Once defined the rod matrices in the GCS, the matrices describing the whole structure have to be built. This step is performed by placing all the element matrices in a global matrix in the proper position according to the GCS. An example of this procedure for a structure discretized in five elements is shown in Figure 2.2.1.1:

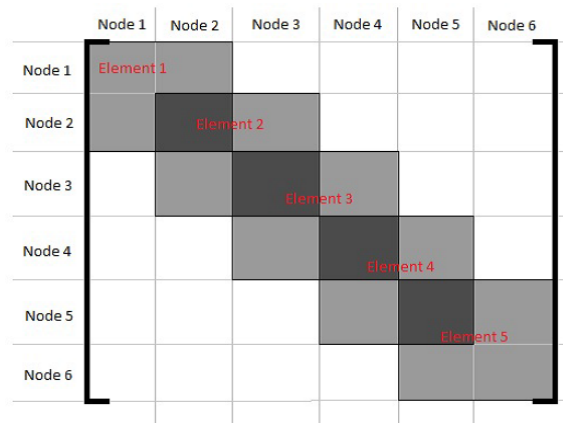


Figure 2.2.1.1: Assembling of global matrices [29].

The next step consists in adding the contributions of the lumped elements defined in the model. Lumped springs and dampers have to be introduced in the matrix: this

is done in the same way as explained for the rod elements, adding their contribution in the position corresponding to the degree of freedom they are acting on.

At the end of this procedure, the system will be described by \mathbf{M}_g , \mathbf{C}_g , \mathbf{K}_g , $g \times g$ real symmetric mass, damping and stiffness matrices and \mathbf{G}_g , $g \times g$ skew-symmetric gyroscopic matrix, where g is the global number of degrees of freedom of the structure.

2.2.2 Application of the constraints

Every rotating system has some constraints applied on it to guarantee the proper motion, which have to be accounted in the finite element model. They are very important not only for the coherent discretization of the model, but in particular because they limit the degrees of freedom of the system in motion and are fundamental to derive the real behaviour of the rotor. The reduction of the degrees of freedom is set up dividing them in *masters* and *slaves* depending if their motion is free or imposed. After that, the same procedure is applied to the nodes, which have to be divided in masters and slaves depending if their motion is free or imposed by other nodes. Then, the constraints can be represented with:

- Rigid Body Elements (RBE) used to link some DOFs between independent nodes to represent constraints, such as hinges, sliders or pins and stored in a matrix \mathbf{T}_{RBE} ;
- Rigid Joint Elements (RJs) used to relate translational and rotational DOFs of nodes which maintain a constant distance in operation and are stored in a matrix \mathbf{T}_{RJs} .

Furthermore, boundary conditions have to be defined for the model, to account for external constraints applied on the structure, and are stored in a matrix \mathbf{T}_{BCs} .

The transformation matrices are condensed in a $n \times g$ matrix \mathbf{T} , where n is the number of active dofs and g is the global number of DOFs, defined in Eq.(2.2.1.1):

$$\mathbf{T} = \mathbf{T}_{RBE} \mathbf{T}_{RJs} \mathbf{T}_{BCs} \quad (2.2.2.1)$$

Then, the matrix is applied on the global matrices as follows:

$$\mathbf{M} = \mathbf{T}^T \mathbf{M}_g \mathbf{T} \quad (2.2.2.2)$$

$$\mathbf{C} = \mathbf{T}^T \mathbf{C}_g \mathbf{T} \quad (2.2.2.3)$$

$$\mathbf{G} = \mathbf{T}^T \mathbf{G}_g \mathbf{T} \quad (2.2.2.4)$$

$$\mathbf{K} = \mathbf{T}^T \mathbf{K}_g \mathbf{T} \quad (2.2.2.5)$$

obtaining the reduced mass, damping, gyroscopic and stiffness matrices of order n , which fully describe the rotor.

In some particular cases a further reduction is required and this is performed applying a Guyan technique, which assumes some nodes to have a displacement that can be computed directly from others. It consists in dividing the nodes in *masters* and *slaves* in the same way as it was done to apply RBE, RJs and BCs, then neglecting inertia forces and external forces applied on slaves. Consequently, the displacement of slaves is computed as a function of the master displacement properly scaled with the stiffness matrix. This method introduces an approximation in the computation, but the error is usually very small if the choice of slave degrees of freedom is appropriate, in fact the inertia forces are not completely neglected, as their contribution is accounted in the kinetic energy as a function of the master.

2.3 Gyroscopic formulation

2.3.1 Conservative and real matrices

The following dynamic problem is considered:

$$\mathbf{M} \ddot{\mathbf{x}} + \Omega \mathbf{G} \dot{\mathbf{x}} + \mathbf{K} \mathbf{x} = \mathbf{0} \quad (2.3.1.1)$$

where:

- \mathbf{M} , \mathbf{K} are real $n \times n$ symmetric matrices describing inertia and stiffness properties;
- \mathbf{G} is a real $n \times n$ skew-symmetric matrix describing gyroscopic properties;
- Ω is a scalar representing the rotational speed;
- \mathbf{x} is a $n \times 1$ vector containing the real coordinates of the nodes.

The eigenproblem results:

$$[\mathbf{K} + i\omega_r\Omega\mathbf{G} - \omega_r^2\mathbf{M}] \boldsymbol{\Psi}_r = \mathbf{0} \quad (2.3.1.2)$$

or

$$\mathbf{K} \boldsymbol{\Psi} = -i\Omega\mathbf{G} \boldsymbol{\Psi} \text{diag}(\omega_r) + \mathbf{M} \boldsymbol{\Psi} \text{diag}(\omega_r^2) \quad (2.3.1.3)$$

with the properties:

- eigenproblem with real and symmetric mass \mathbf{M} and stiffness \mathbf{K} matrices, with real and skew-symmetric gyroscopic matrix \mathbf{G} ;
- purely imaginary non-conjugate eigenvalues \mathbf{S}_r and complex non-conjugate eigenvectors $\boldsymbol{\Psi}_r$. There may be null eigenvalues if $\det(\mathbf{K}) = 0$

This is a second order problem in ω_r , so it is computationally convenient to solve the equivalent first order problem using Duncan formulation.

This method consists in rearranging the terms of Eq. (2.3.1.1) in a particular state space form, passing from a system of n second order equations to a system of $2n$ first order equations, where n is the number of degrees of freedom of the structure.

The dynamic problem is reduced to:

$$\mathbf{A}\dot{\mathbf{y}} + \mathbf{B}\mathbf{y} = \tilde{\mathbf{f}} \quad (2.3.1.4)$$

where:

- \mathbf{y} , $\dot{\mathbf{y}}$ are respectively the generalised displacements and velocities $2n \times 1$ of the first order problem

$$\mathbf{y} = \begin{Bmatrix} \mathbf{x} \\ \dot{\mathbf{x}} \end{Bmatrix}, \dot{\mathbf{y}} = \begin{Bmatrix} \dot{\mathbf{x}} \\ \ddot{\mathbf{x}} \end{Bmatrix} \quad (2.3.1.5)$$

- \mathbf{A} is a $2n \times 2n$ real, symmetric and indefinite matrix

$$\mathbf{A} = \begin{bmatrix} \Omega\mathbf{G} & \mathbf{M} \\ \mathbf{M} & \mathbf{0} \end{bmatrix} \quad (2.3.1.6)$$

- \mathbf{B} is a $2n \times 2n$ real, symmetric and indefinite matrix

$$\mathbf{B} = \begin{bmatrix} \mathbf{K} & \mathbf{0} \\ \mathbf{0} & -\mathbf{M} \end{bmatrix} \quad (2.3.1.7)$$

- $\tilde{\mathbf{f}}$ is the generalised force vector $2n \times 1$;
- the second block of equations of Eq. (2.3.1.4) is the identity:

$$\mathbf{M}\dot{\mathbf{x}} - \mathbf{M}\dot{\mathbf{x}} = 0 \quad (2.3.1.8)$$

Neglecting static generalised external forces, Eq. (2.3.1.4) results:

$$\mathbf{A}\dot{\mathbf{y}} + \mathbf{B}\mathbf{y} = 0 \quad (2.3.1.9)$$

To evaluate a non-null stationary oscillating behaviour, a generalised exponential solution is assumed:

$$\mathbf{y} = \mathbf{y}_0 e^{St} \quad (2.3.1.10)$$

$$\dot{\mathbf{y}} = S\mathbf{y}_0 e^{St} \quad (2.3.1.11)$$

since time is separable and erasable from the equation:

$$(\mathbf{B} + S\mathbf{A}) \mathbf{y}_0 e^{St} = \mathbf{0} \quad (2.3.1.12)$$

$$(\mathbf{B} + S\mathbf{A}) \mathbf{y}_0 = \mathbf{0} \quad (2.3.1.13)$$

Beside the trivial solution

$$\mathbf{y}_0 = \mathbf{0}$$

that corresponds to the static non deformed condition, the eigenproblem can be solved to find the eigenvalues vector and the eigenvectors matrix:

$$(\mathbf{B} + S_r\mathbf{A}) \left\{ \tilde{\Psi}_r \right\} = \{0\} \quad (2.3.1.14)$$

finding the non-null solutions by means of:

$$\det(\mathbf{B} + S_r\mathbf{A}) \left\{ \tilde{\Psi}_r \right\} = 0 \quad (2.3.1.15)$$

From the equation, the eigenvalues are obtained:

$$S = \mathbf{S}_r = [S_1, S_2, \dots, S_{2r}]^T \quad (2.3.1.16)$$

then for each obtained eigenvalue, Eq. (2.3.1.14) can be solved obtaining the related complex eigenvector space:

$$\tilde{\Psi} = \left[\left\{ \tilde{\Psi}_1 \right\}, \left\{ \tilde{\Psi}_2 \right\}, \dots, \left\{ \tilde{\Psi}_{2r} \right\} \right] \quad (2.3.1.17)$$

Where the relationship between the complete eigenvector $\tilde{\Psi}$ and the first half Ψ and the corresponding eigenvalues S_r is:

$$\tilde{\Psi} = \begin{bmatrix} \Psi \\ \Psi \text{diag}(S_r) \end{bmatrix} \quad (2.3.1.18)$$

The gyroscopic matrix has a stiffening effect on the structure, having important repercussions on the stability. In particular the system is:

- *marginally stable* if $\det(\mathbf{K}) > 0$ independently on the magnitude of \mathbf{G} ;
- *unstable* if $\det(\mathbf{K}) < 0$.

2.3.2 Classical dissipative and real matrices

The following dynamic problem is considered:

$$\mathbf{M} \ddot{\mathbf{x}} + (\mathbf{C} + \Omega \mathbf{G}) \dot{\mathbf{x}} + \mathbf{K} \mathbf{x} = \mathbf{0} \quad (2.3.2.1)$$

where:

- \mathbf{M} , \mathbf{C} , \mathbf{K} are real $n \times n$ symmetric matrices describing inertia, damping and stiffness properties;
- \mathbf{G} is a real $n \times n$ skew-symmetric matrix describing gyroscopic properties;
- Ω is a scalar representing the rotational speed;
- \mathbf{x} is a $n \times 1$ vector containing the real coordinates of the nodes.

The eigenproblem results:

$$[\mathbf{K} + i\omega_r(\mathbf{C} + \Omega \mathbf{G}) - \omega_r^2 \mathbf{M}] \Psi_r = \mathbf{0} \quad (2.3.2.2)$$

or

$$\mathbf{K} \Psi = -i(\mathbf{C} + \Omega \mathbf{G}) \Psi \text{diag}(\omega_r) + \mathbf{M} \Psi \text{diag}(\omega_r^2) \quad (2.3.2.3)$$

with the properties:

- eigenproblem with real and symmetric mass \mathbf{M} , damping \mathbf{C} and stiffness \mathbf{K} matrices, with real and skew-symmetric gyroscopic matrix \mathbf{G} ;

- complex and non-conjugate eigenvalues \mathbf{S}_r and complex and non-conjugate eigenvectors Ψ_r .

This is a second order problem in ω_r , so it is computationally convenient to solve the equivalent first order problem using Duncan formulation.

This method consists in rearranging the terms of Eq. (2.3.2.1) in a particular state space form, passing from a system of n second order equations to a system of $2n$ first order equations, where n is the number of degrees of freedom of the structure.

The dynamic problem is reduced to:

$$\mathbf{A}\dot{\mathbf{y}} + \mathbf{B}\mathbf{y} = \tilde{\mathbf{f}} \quad (2.3.2.4)$$

where:

- \mathbf{y} , $\dot{\mathbf{y}}$ are respectively the generalised displacements and velocities $2n \times 1$ of the first order problem

$$\mathbf{y} = \begin{Bmatrix} \mathbf{x} \\ \dot{\mathbf{x}} \end{Bmatrix}, \dot{\mathbf{y}} = \begin{Bmatrix} \dot{\mathbf{x}} \\ \ddot{\mathbf{x}} \end{Bmatrix} \quad (2.3.2.5)$$

- \mathbf{A} is a $2n \times 2n$ real, symmetric and indefinite matrix

$$\mathbf{A} = \begin{bmatrix} \mathbf{C} + \Omega\mathbf{G} & \mathbf{M} \\ \mathbf{M} & \mathbf{0} \end{bmatrix} \quad (2.3.2.6)$$

- \mathbf{B} is a $2n \times 2n$ real, symmetric and indefinite matrix

$$\mathbf{B} = \begin{bmatrix} \mathbf{K} & \mathbf{0} \\ \mathbf{0} & -\mathbf{M} \end{bmatrix} \quad (2.3.2.7)$$

- $\tilde{\mathbf{f}}$ is the generalised force vector $2n \times 1$;
- the second block of equations of Eq. (2.3.2.4) is the identity:

$$\mathbf{M}\dot{\mathbf{x}} - \mathbf{M}\dot{\mathbf{x}} = 0 \quad (2.3.2.8)$$

Neglecting static generalised external forces, Eq. (2.3.2.4) results in:

$$\mathbf{A}\dot{\mathbf{y}} + \mathbf{B}\mathbf{y} = 0 \quad (2.3.2.9)$$

Then, following the same procedure as in Sec. (2.3.1) the eigenvalue problem can be solved to find the eigenvalues \mathbf{S}_r and the eigenvectors Ψ .

For a classical damped gyroscopic system, the eigenvalues \mathbf{S}_r are complex non-conjugate, leading to complex non-conjugate eigenvectors Ψ . Moreover, damping plays an important role in the nature of eigenvalues because more than changing the imaginary part, it affects the real part, making it different in a couple of frequencies.

It is important to remark that a system which shows to be stable for $\mathbf{C} = \mathbf{0}$ and $\mathbf{G} = \mathbf{0}$, marginally stable according to the previous definition, still keeps its stability after the introduction of arbitrary gyroscopic and dissipative forces.

Chapter 3

Testbench

3.1 Description of the parametric test-rig

The parametric test-rig, of which a 3D FE model is built, is shown in Figure 3.1.1:

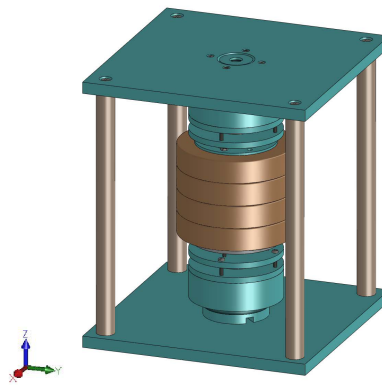


Figure 3.1.1: Model of vertical magnetic rotor.

A magnetic rotor is a rotating structure in which the traditional cylindrical bearings are substituted by magnetic supports. These devices are able to sustain moving parts without physical contact and their functioning principle is based on the laws of electromagnetism.

Moreover, similarly to conical rolling bearings, magnetic supports are able to produce forces in all directions in space, the intensity of which depends not only on the material they are made of, but also on the quantity and position of the rings.

In the case study, the magnetic rotor has supporting bearings made of an alloy of neodymium, iron and boron. The choice of these permanent magnets is due to the fact that they are the strongest commercially available, although they are still relatively fragile and can be easily damaged.

One of the peculiarities of this magnetic rotor is the minimum contribution of weight force on the vertical axis. This situation takes place because the stator rings produce two axial magnetic forces on the rotor rings that are in the opposite direction with respect to weight, pushing up the whole rotor.

In order to obtain a relevant reduction of the weight on the thrust bearing, it is necessary to work on axial instability and radial stability. The decrease of the weight of the rotor on the floor is an important goal to achieve, since it results in lower resistance actions, developed at the base. Friction does not occur in any location of the structure, thanks to the absence of lubricant and of physical contact of the parts, so it is fundamental to reduce it as much as possible in the contact point with the thrust bearing.

The rotor is composed by the main shaft, made of an aluminium alloy, that shows characteristic stiffness properties to be considered a rigid body. The mass distribution is not homogeneous due to the presence of a flange, required for the mounting of the brass hubs. These discs are positioned in the middle of the shaft and represent the mass of the assembly, their material is properly chosen to avoid the generation of eddy current in operating conditions.

The weight of the structure is only partially reduced by the magnetic bearings so, as previously mentioned, a thrust bearing is required along the vertical direction. This task is covered by a sapphire, material with a high hardness (9 on the Mohs scale), which is positioned on the base of the structure.

The stator structure sustaining the rotor is made of polytetrafluoroethylene (PTF), commonly known as Teflon. Its diamagnetic behaviour shows the Teflon to be suitable for the application, in order to avoid magnetic interaction with the rotor.

As it will be discussed more in details in Sec. (3.1.1) and Sec. (3.1.2), there are many possible configurations of the structure. The analysis developed in this thesis refers to one particular configuration with four hubs and six magnets on the vertical rotor, two

positioned on the upper side of the discs and four on the lower side. This choice is a trade off to have coherence with the decision to work in axial instability and with a force pointing upwards. This arrangement of the rotor is shown in Figure 3.1.2:



Figure 3.1.2: Rotor with four hubs and six magnets.

Number of magnets	Mass [kg]	Barycentre [m]	Moments of inertia [kg m ²]		
6	4.798	X Y Z	$6.677 \cdot 10^{-3}$	0	0
		0 0 -0.04	0	$6.677 \cdot 10^{-3}$	0
			0	0	$6.509 \cdot 10^{-3}$

Table 3.1.1: Characteristics of the rotor in the chosen configuration.

3.1.1 Inertial properties

As it was stated in the description of the test rig, the inertial properties of the whole structure strongly depend on the brass hubs. The particular of one disc is shown in Figure (3.1.1.1) and the geometrical and inertia properties are summarised in Table (3.1.1.1):

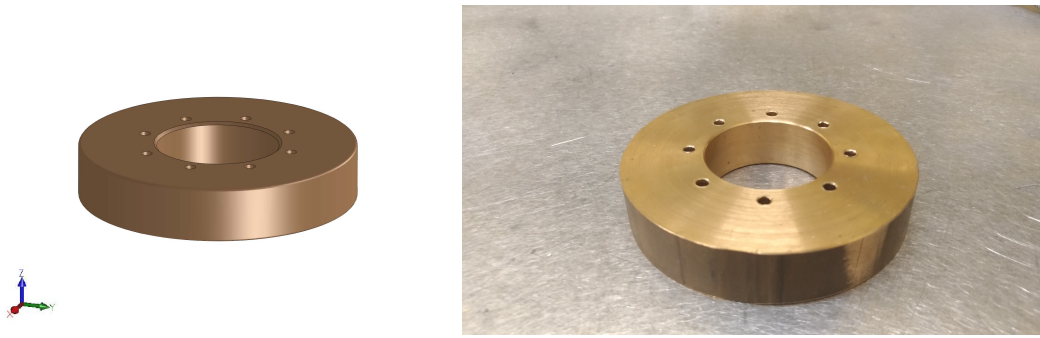


Figure 3.1.1.1: Particular of a brass hub.

Characteristic	Property	Value
Hub Geometry	ϕ_{ext} external diameter [mm]	100
	ϕ_{int} internal diameter [mm]	44
	t thickness [mm]	20
Hub Material	ρ density [kg/m^3]	8500
	E Young modulus [GPa]	100
	ν Poisson ratio [-]	0.35

Table 3.1.1.1: Hub geometric and material characteristics.

The flange of the rotating shaft allows the correct mounting of a number of brass hubs up to four. This results in the fact that with one bench it is possible to study different configurations by just changing the number of masses.

Increasing the number of brass hubs leads to a lowering of the position of the structure barycentre and has a high influence on the weight, since each disc has a mass $m=1.052\text{kg}$. Moreover, the resultant moments of inertia change according to the quantity of discs present, so the rotating behaviour is very different in the configuration with no masses with respect to the maximum weight.

However, there is also the possibility to locate, instead of the brass hubs, discs made of a different material, holding the same insulation properties. Many studies can be conducted with the same test bench only changing the central masses.

3.1.2 Magnetic supports

The passive magnetic bearings are located in the upper and lower side of the brass hubs. It is possible to distinguish rotoric rings, mounted on the shaft, and statoric rings, mounted on the non rotating support. They are silver-white rings, of which a particular is shown in Figure (3.1.2.1) and a summary of the geometrical and magnetic properties is reported in Table (3.1.2.1).

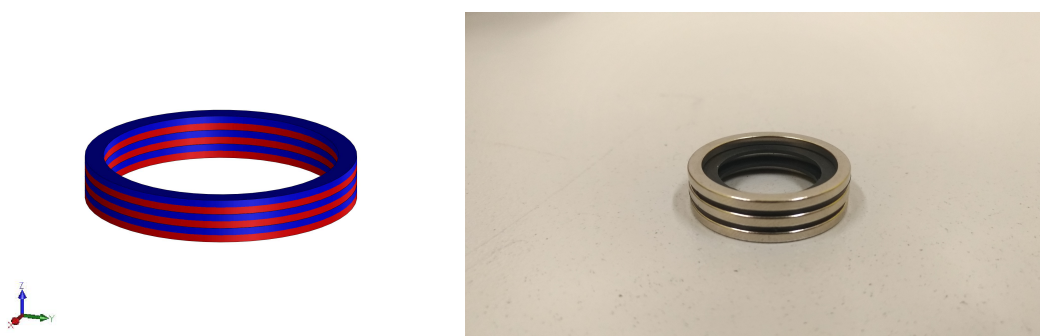


Figure 3.1.2.1: Particular of magnetic rings.

Characteristic	Property	Value
Geometry 1-Statoric rings	$2h$ height along z magnetization axis[mm]	2
	ϕ_{ext} external diameter[mm]	37
	ϕ_{int} internal diameter[mm]	32
Geometry 2-Rotoric rings	$2h$ height along z magnetization axis[mm]	2
	ϕ_{ext} external diameter[mm]	29.5
	ϕ_{int} internal diameter[mm]	24.5
Material	B_r residual magnetic induction [T]	1.2

Table 3.1.2.1: Geometric and material characteristics of the rings.

The number of magnets and the reciprocal position of stator and rotor rings strongly influence the stability of the system and the amount of weight that can be counter-balanced. These two parameters affect the intensity of the forces that are generated on the rotor and their direction of action. Consequently, it is possible to use the same structure to analyse the behaviour in operating conditions for different configurations, changing the number of rings and their position.

3.2 3D finite element model

The rotating system described in Sec. (3.1) is discretised in a series of rod elements. The vertical elements are connected one to the other with rigid joints to impose a coherent displacement of the consecutive nodes. The thrust bearing supporting the bottom part of the rotor is modelled as an elastic element with a proper spring stiffness, positioned in the node corresponding to the base. The magnetic bearings are accounted in the model for their elastic and dissipative contributions. Two elastic elements for each support are located in the related nodes for the translational and transversal degrees of freedom. Three damping elements for each support are located in the related nodes for the transversal and torsional degrees of freedom.

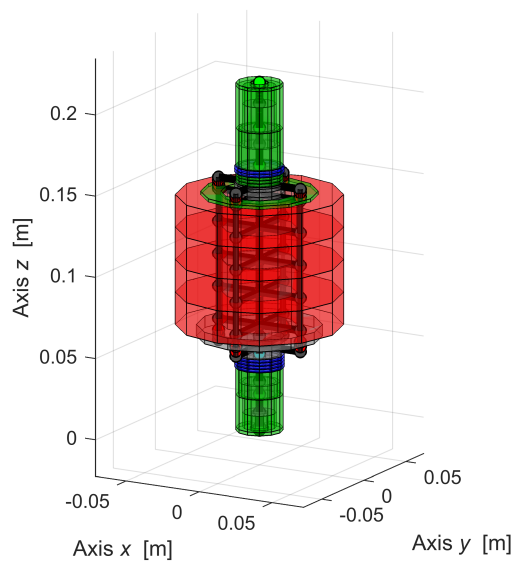


Figure 3.2.1: 3D model of the rotor on magnetic supports.

The 3D model contains 111 nodes, each of them defined by 6 degrees of freedom. This would result in a very large number of equations to solve, but it can be cut down with the application of the constraints on the elements as explained in Sec. (2.2). Since the rotor is rigid, the reduction applied to the model leads to a 6 degrees of freedom expression, 3 translational and 3 rotational.

The discretised structure of the rigid shaft is shown in Figure 3.2.2:

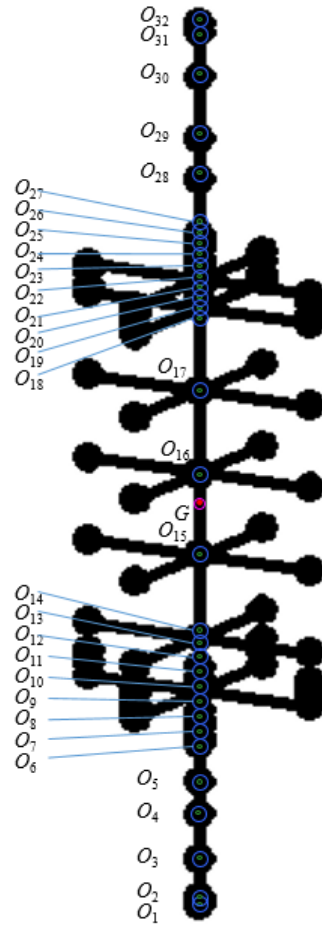


Figure 3.2.2: Nodes of the discretised rigid shaft and barycentre G .

Consequently, the dynamic problem for the rotor is:

$$\mathbf{M} \ddot{\mathbf{x}} + (\mathbf{C} + \Omega \mathbf{G}) \dot{\mathbf{x}} + \mathbf{K} \mathbf{x} = \mathbf{0} \quad (3.2.1)$$

where the matrices obtained with a Timoshenko approach are:

- \mathbf{M} , \mathbf{C} , \mathbf{K} are real 6×6 symmetric matrices describing inertia, damping and stiffness properties;

$$\mathbf{M} = \begin{bmatrix} 4.7963 & 0 & 0 & 0 & 1.5524 \cdot 10^{-4} & 0 \\ 0 & 4.7963 & 0 & 1.5524 \cdot 10^{-4} & 0 & 0 \\ 0 & 0 & 4.7963 & 0 & 0 & 0 \\ 0 & 1.5524 \cdot 10^{-4} & 0 & 0.0068 & 0 & 0 \\ 1.5524 \cdot 10^{-4} & 0 & 0 & 0 & 0.0068 & 0 \\ 0 & 0 & 0 & 0 & 0 & 0.0065 \end{bmatrix} \quad (3.2.2)$$

$$\mathbf{C} = \begin{bmatrix} 0.004 & 0 & 0 & 0 & -9.6 \cdot 10^{-6} & 0 \\ 0 & 0.004 & 0 & 9.6 \cdot 10^{-6} & 0 & 0 \\ 0 & 0 & 0 & 0 & 0 & 0 \\ 0 & 9.6 \cdot 10^{-6} & 0.13947 \cdot 10^{-5} & 0 & 0 & 0 \\ -9.6 \cdot 10^{-6} & 0 & 0 & 0 & 1.3947 \cdot 10^{-5} & 0 \\ 0 & 0 & 0 & 0 & 0 & 4 \cdot 10^{-5} \end{bmatrix} \quad (3.2.3)$$

$$\mathbf{K} = \begin{bmatrix} 14200 & 0 & 0 & 0 & -104.88 & -1.4943 \cdot 10^{-12} \\ 0 & 14200 & 0 & 104.88 & 0 & 0 \\ 0 & 0 & 1 \cdot 10^7 & 2.3432 \cdot 10^{-10} & 0 & 0 \\ 0 & 104.88 & 2.3432 \cdot 10^{-10} & 49.8518 & 0 & 0 \\ -104.88 & 0 & 0 & 0 & 49.8518 & 2.5002 \cdot 10^{-14} \\ -1.4943 \cdot 10^{-12} & 0 & 0 & 0 & 2.5002 \cdot 10^{-14} & -8.6644 \cdot 10^{-10} \end{bmatrix} \quad (3.2.4)$$

- \mathbf{G} is a real 6×6 skew-symmetric matrix describing gyroscopic properties;

$$\mathbf{G} = \begin{bmatrix} 0 & 0 & 0 & 0 & 0 & 0 \\ 0 & 0 & 0 & 0 & 0 & 0 \\ 0 & 0 & 0 & 0 & 0 & 0 \\ 0 & 0 & 0 & 0 & 0.0065 & 0 \\ 0 & 0 & 0 & -0.0065 & 0 & 0 \\ 0 & 0 & 0 & 0 & 0 & 0 \end{bmatrix} \quad (3.2.5)$$

- Ω is a scalar representing the rotational speed;
- \mathbf{x} is a 6×1 vector containing the real coordinates of the master node.

The model, tested at a rotational speed $\Omega = 300$ rad/s is solved with the procedure explained in Sec. (2.2) and shows twelve natural frequencies at which correspond:

- 2 undamped conjugate imaginary modes;
- 8 complex conjugate underdamped modes;
- 2 overdamped modes.

The eigenvalues and eigenvectors are double with respect to the six degrees of freedom of the rotor, due to the resolution of the problem with the Duncan method. This numerical result has no influence on the description of the real behaviour of the rotor, because only six modes are independent of the twelve modes resulting from the analysis.

As expected from rigid body theory of a rotating cylinder, the modes are two conical motions, two cylindrical, one shaking of the base and the rotation of the rotor around its axis.

Chapter 4

Numerical results

The simulation on the parametric test rig can be run at different spin speed to see how it will behave in the experimental analysis. The model described in the previous section is tested and the results in terms of modal shapes are presented. The assumption of rigid rotor is reasonable if it has to operate at speeds lower than half the first critical speed, while the more it gets closer to this velocity the higher is the possibility that it will deflect. A further step to have a complete overview of the behaviour is done by building a flexible finite element model of the rotor.

4.1 Rigid model

The analysis of the rigid rotor modelled in Sec. (3.2) leads to the prediction of natural frequencies of the system and modal shapes. In this section are presented the results obtained from the test of the rigid magnetic rotor at a spin speed $\Omega = 300$ rad/s are presented. As expected from rigid body theory of a rotating cylinder, the modes are two conical motions, two cylindrical, one shaking of the base and the rotation of the rotor around its axis.

The two low frequency modes, taking place at $S = 4.184$ Hz, describe the same conical shape. Mode 1 is a counter clockwise rotation, while Mode 2 is a clockwise rotation. They are reported in Figure (4.1.1).

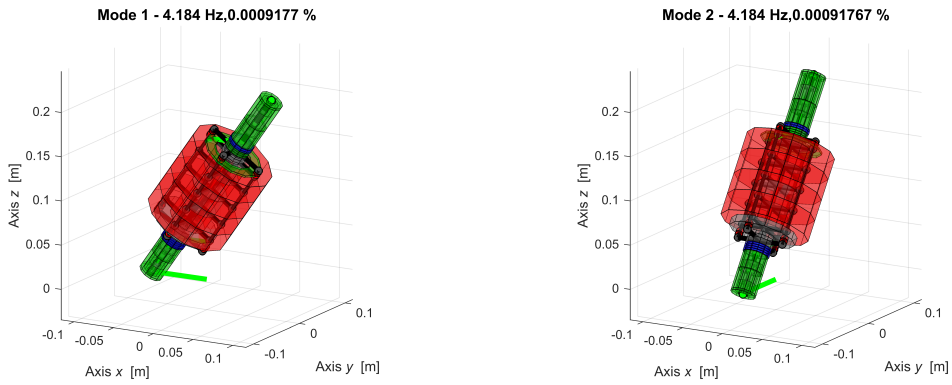


Figure 4.1.1: Conical modes at low frequency.

The four cylindrical modes take place at two frequencies that are almost coincident. They are reported in Figure (4.1.2) and Figure (4.1.3).

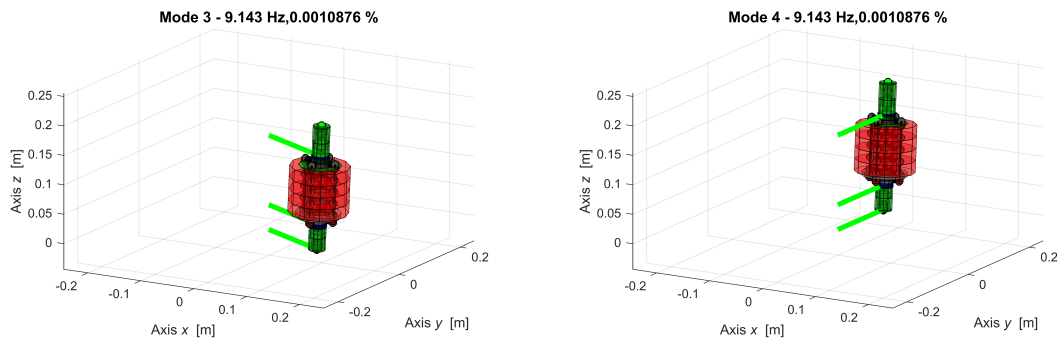


Figure 4.1.2: Bounce modes at $S = 9.143$ Hz.

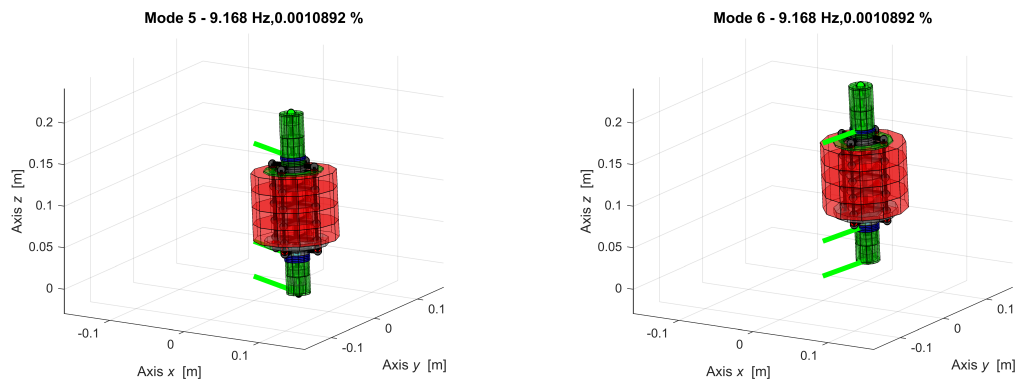


Figure 4.1.3: Bounce modes at $S = 9.168$ Hz.

The two high frequency modes, taking place at $S = 49.06$ Hz, describe the same conical shape. Mode 7 is a clockwise rotation, while Mode 8 is counter clockwise. They are reported in Figure (4.1.4).

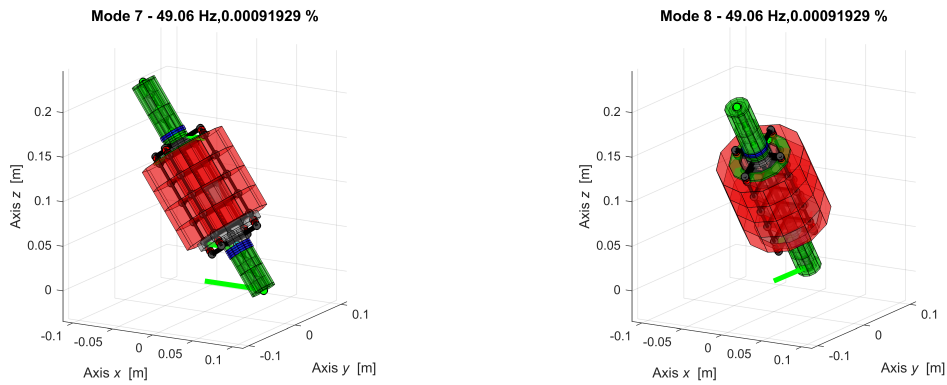


Figure 4.1.4: Conical modes at high frequency.

The undamped modes taking place at $S = 229.8$ Hz are the shaking of the base due to the presence of the thrust bearing, they are shown in Figure (4.1.5).

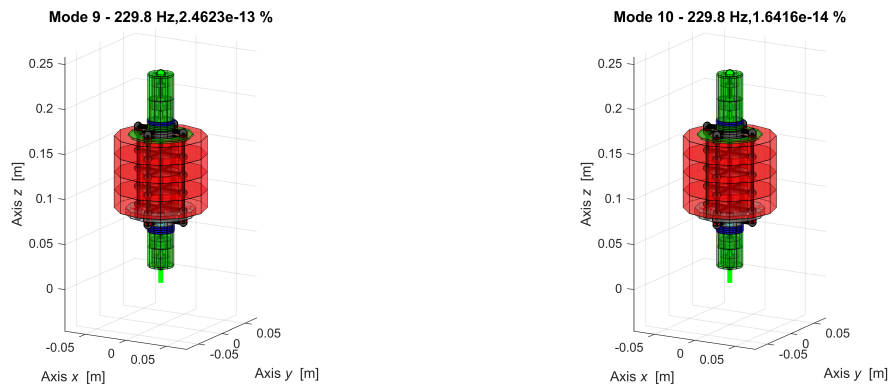


Figure 4.1.5: Shaking modes.

The two overdamped modes, both taking place at around $S = 0$ Hz, describe the rigid body motion of the rigid rotor around its axis. They are reported in Figure (4.1.6).

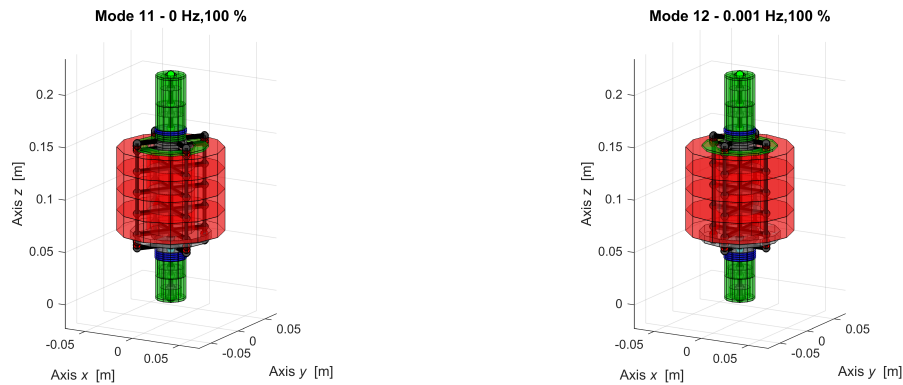


Figure 4.1.6: Rigid body modes.

4.2 Flexible model

A 3D finite element model of the flexible rotor is built starting from the rigid one presented in Sec. (3.2). As previously explained, the main aluminium rotor is modelled subdividing it in rod elements, which have a proper rigidity given by the material. These elements are connected one to that following by rigid joints, that make it possible to model the whole shaft.

In order to derive a flexible model from this previous work, it is possible to change the constitutive material of the rod elements and remove the rigid joints imposed on the shaft.

In the work described in this thesis, it was decided to remove the rigidity constraints and change the Young modulus of the material to better visualise the characteristic modes, ending with a model presented in Figure (4.2.1).

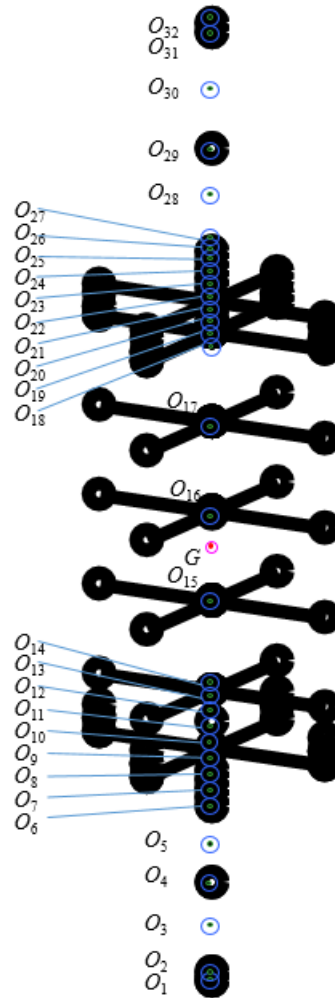


Figure 4.2.1: Nodes of the discretised flexible shaft and barycentre G .

This model is closer to the actual behaviour of a rotating structure, because no real system is purely rigid. The deformability of the shaft leads to have 240 degrees of freedom describing the structure. The dynamic problem is solved following the same procedure discussed in Sec. (2.3), resulting in the identification of 480 modal shapes. By sorting them in increasing order of their relative eigenvalue, it is possible to state that the first twelve modes are referred to rigid motions, while at higher frequencies the flexible modal shapes occur. The characteristic flexible shapes of the model tested at a spin speed $\Omega = 300$ rad/s are presented.

The six modes, taking place at frequencies that are almost coincident, describe the first flexible shape and are reported in Figure (4.2.2), Figure (4.2.3) and Figure (4.2.4).

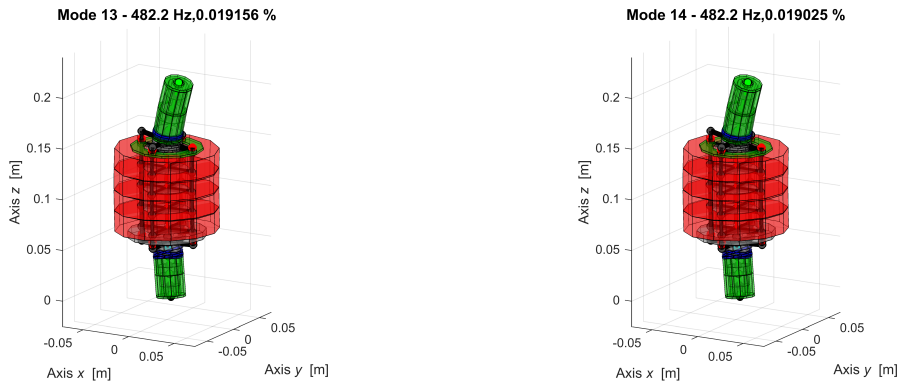


Figure 4.2.2: First flexible modes at $S = 482.2$ Hz.

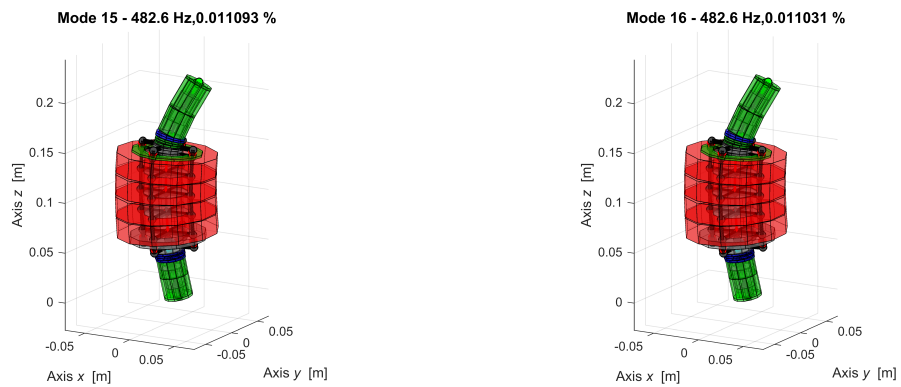


Figure 4.2.3: First flexible modes at $S = 482.6$ Hz.

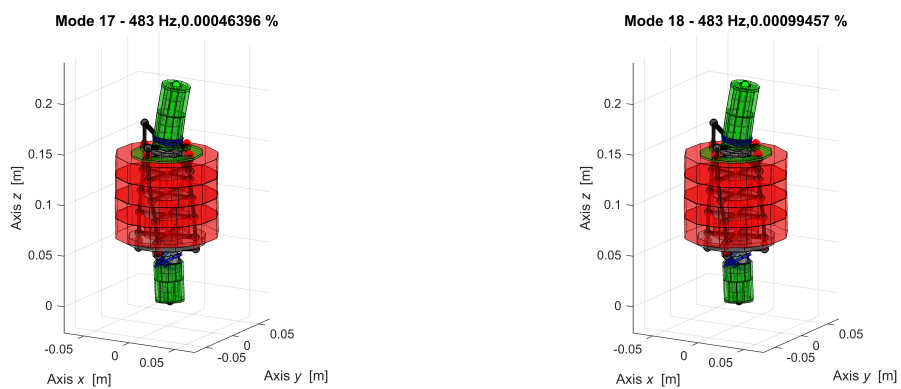


Figure 4.2.4: First flexible modes at $S = 483$ Hz.

The modes taking place at $S = 607.9$ Hz, describe second flexible shape and they are reported in Figure (4.2.5).

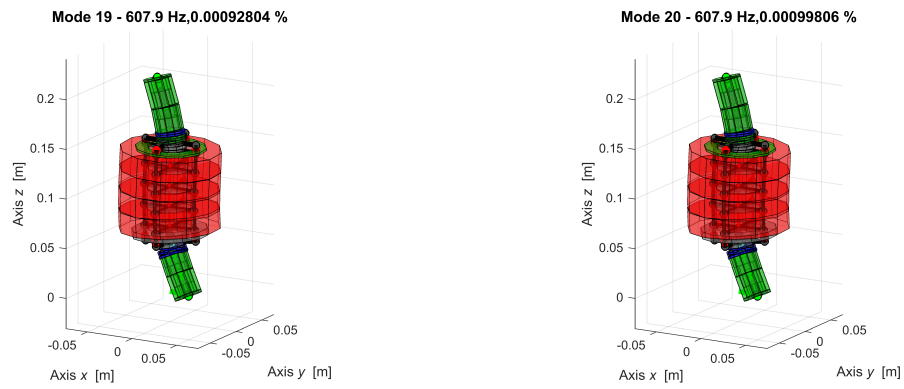


Figure 4.2.5: Second flexible modes at $S = 607.9$ Hz.

4.3 Comparison

The analysis of the 3D FE model is performed in real coordinates at different rotating speeds, obtaining the evolution of the natural frequencies as expected from the theory of a rigid rotor. It is derived the Campbell diagram showing the variation of the eigenvalues modulus in the range of spin speed $\Omega = 0 \div 314$ rad/s. The comparison between the graph known in literature and the one obtained from the numerical procedure is presented in Figure (4.3.1) and Figure (4.3.2). In the numerical Campbell diagram, the modes related to shaking of the base are not reported because they are referring to the specific case study and cannot be compared with the general diagram of a four degrees of freedom rotor.

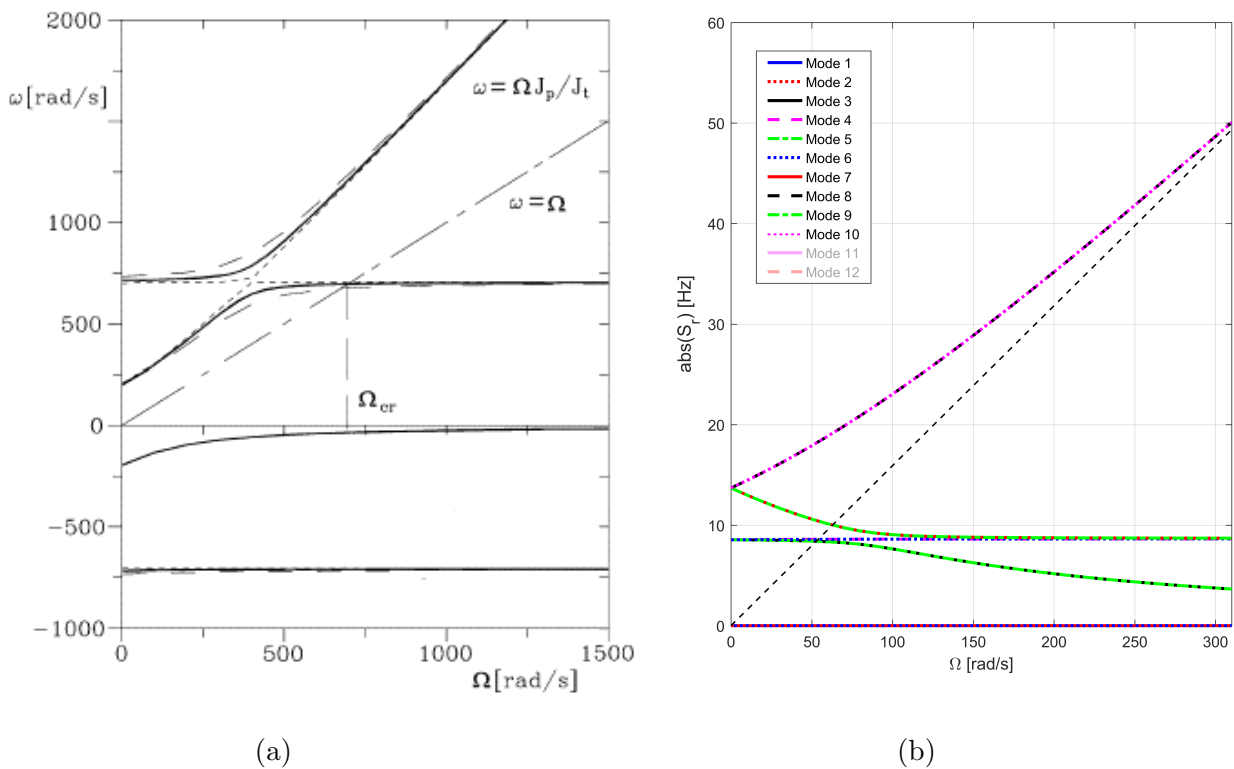


Figure 4.3.1: 4 degrees of freedom rotor [1] (a) and 3D rigid model (b).

The 3D rigid model shows to be reliable since the eigenvalues referred to rigid body motions are similar to those obtained for the four degrees of freedom rotor model.

Once determined the validity of the rigid model, the analysis is extended to the flexible

one, which is tested in the range of spin speed $\Omega = 0 \div 314$ rad/s. The Campbell diagram for the flexible model is derived and the comparison with the rigid rotor diagram is proposed in Figure (4.3.3) and Figure (4.3.4).

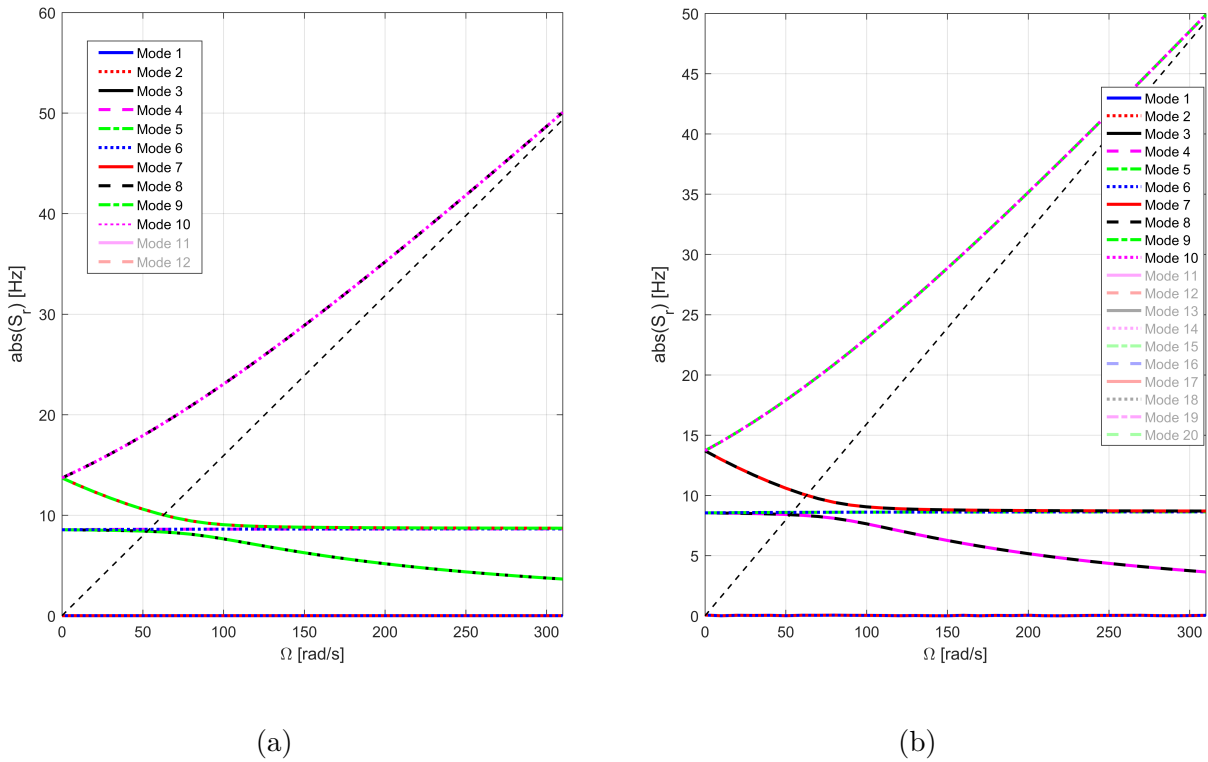


Figure 4.3.2: (a) 3D rigid model and (b) 3D flexible model.

The Campbell diagram of the flexible rotor is reduced to the first ten modes, since they are comparable with the rigid motions. Flexible modes take place at increasingly high frequencies and they are not influenced by rotating speed, consequently they correspond to horizontal lines in the diagram above.

The stability of the system can be analysed looking at the evolution of the real part of the eigenvalues at increasing speed. As explained in Sec. (1.2), the real part of the eigenvalue determines how the structure, in terms of amplitude of the orbit, behaves at that rotating speed.

The diagrams for rigid and flexible model are reported in Figure (4.3.5) and Figure (4.3.6).

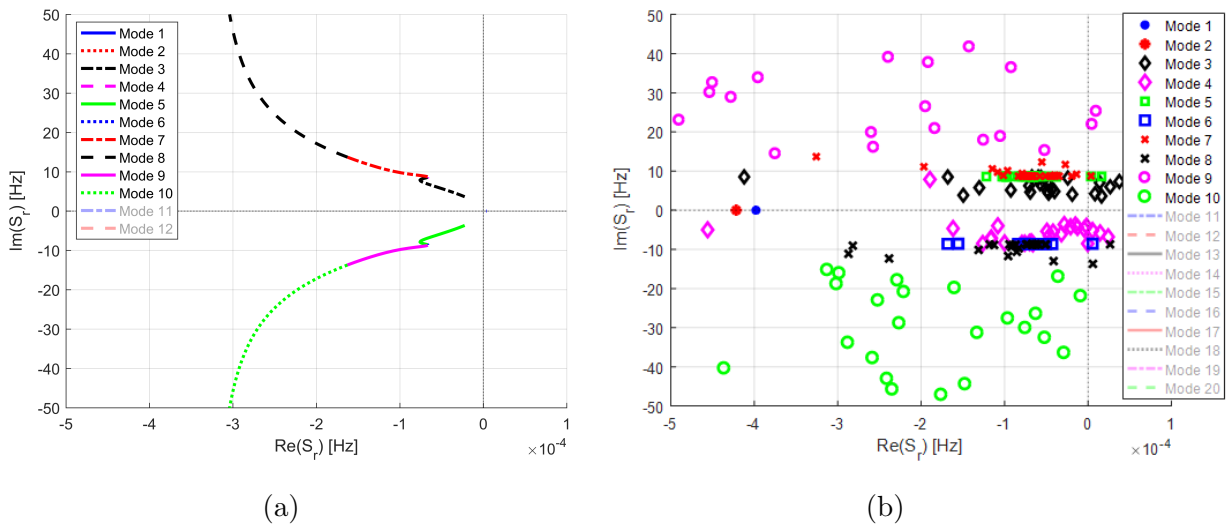


Figure 4.3.3: Stability for the rigid (a) and flexible (b) rotor.

Both the rigid and the flexible rotor show to be stable in a wide range of velocities, because the real part of the eigenvalues stays negative. In only a small part of the diagram the real part of the eigenvalues becomes positive, but the range is so restricted and the values it assumes are of the order of 10^{-4} , that it could be attributable to numerical imprecision.

Conclusions

This work presents a procedure to perform the gyroscopic analysis with FEM of a rotor on magnetic supports. As a case study, it was developed a 3D rigid finite element model of a parametric test rig, already designed and built. The results obtained are aligned with those present in the literature for a four degrees of freedom model. In particular, here it is proposed the comparison between the Campbell diagrams for the analytical and numerical case, to show the similarities in the evolution of eigenvalues with increasing spin speed. Due to the validity of the rigid model and starting from this, a 3D flexible finite element model is build, removing the simplifying assumptions made on the rigidity of the flywheel. The resulting analysis is closer to the real behaviour of the rotor since, in addition to the rigid body modes, it considers the flexible modes occurring at higher frequencies. The Campbell diagrams for the rigid and flexible model are compared, showing that they are matching for the modes describing the rigid behaviour. Stability is investigated for the two configurations: it is possible to state that the system is stable for a large range of working speeds, while further studies are suggested to determine the threshold. Based on the results obtained in the present study, the model is suitable to predict the behaviour of the flywheel during experimental tests that are planned in the next future.

Reference

- [1] Genta G., *Vibration dynamics and control*, Springer, New York, New York, 1997.
- [2] Rankine W.J.M., “On the centrifugal force of rotating shafts”, *The Engineer*, 1869.
- [3] Dunkerley S., “On the whirling and vibration of shafts”, *Proceedings of the Royal Society of London*, 54, 1893, pp. 365–370.
- [4] Föppl A., “Das problem der lavalschen turbinenwelle”, *Der Civilingenieur*, 4, 1895, pp. 335-342.
- [5] Jeffcott H., “The lateral vibration of loaded shafts in the neighbourhood of a whirling speed - the effect of want of balance”, *Philosophical Magazine*, Vol 37(6), 1919, pp. 301-314.
- [6] Meirovitch L., *Fundamentals of vibrations*, McGraw-Hill, New York, New York, 2001.
- [7] Timoshenko S.P., “On the correction factor for shear of the differential equation for transverse vibrations of bars of uniform cross-section”, *Philosophical Magazine*, 1921, pp. 744.
- [8] Myklestad N. O., “A new method of calculating natural modes of uncoupled bending Vibration of airplane wings and other types of beams”, *Journal of the Aeronautical Sciences (Institute of the Aeronautical Sciences)*, 11(2), 1944, pp 153–162.
- [9] Prohl M.A., “A general method for calculating critical speeds of flexible rotors”, *Trans. ASME*, 66, 1945, pp. A-142–148.

-
- [10] Ruhl R.L., *Dynamic of distributed parameter rotor systems: transfer matrix and finite element techniques*, PhD dissertation, Cornell University, 1970.
- [11] Ruhl R.L, Booker J.F., “A finite element model for distributed parameter turborotor systems”, *ASME Journal of Engineering for Industry*, 94(1), 1972, pp 128-132.
- [12] Thorkildsen T., “Solution of a distributed mass and unbalanced rotor system using a consistent mass matrix approach”, *MSE Engineering Report*, Arizona State University, 1972.
- [13] Polk S.R., “Finite element formulation and solution of flexible rotor-rigid disc systems for natural frequencies and critical whirl speed”, *MSE Engineering Report*, Arizona State University, 1974.
- [14] Nelson H.D., McVaugh J.M., “The dynamics of rotor-bearing systems using finite elements”, *ASME Journal of Engineering for Industry*, 98(2), 1976, pp 593-600.
- [15] Zorzi E.S., Nelson H.D., “Finite element simulation of rotor-bearing systems with internal damping”, *ASME Journal of Engineering for Power*, 99(1), 1977, pp 71-76.
- [16] Dimarogonas A.D., “A general method for stability analysis of rotating”, *Ingenieur - Archive*, 44(1), 1975, pp. 9-20.
- [17] Gasch R., “Vibration of large turbo-rotors in fluid film bearings on an elastic foundation”, *Journal of Sound and Vibration*, 47(1), 1976, pp. 53-73.
- [18] Nelson H. D., “A finite rotating shaft element using Timoshenko beam theory”, *ASME Journal of Mechanical Design*, 102, 1980, pp. 793-803.
- [19] Duncan W.J., *Mechanical admittances and their applications to oscillation problems*, H.M.S.O., London, England, 1947.
- [20] Frazer R.A., Duncan W.J., Collar R.A., *Elementary matrices*, Cambridge University Press, Cambridge, England, 1957.
- [21] Lancaster P., *Lambda-Matrices and Vibrating Systems*, Pergamon Press, Oxford, England, 1966.
- [22] Meirovitch L., and Nelson, H. D., “On the High-Spin Motion of a Satellite Containing Elastic Parts”, *Journal of Spacecraft and Rockets*, 3(11), 1966, pp. 1958-1602.
-

-
- [23] Meirovitch L., “A new method of solution of the eigenvalue problem for gyroscopic systems”, *Aiaa Journal*, 12(10), 1974, pp. 1337-1342.
- [24] Lancaster P., “Stability of linear gyroscopic systems: A review” *Linear Algebra and its Applications*, 439, 2013, pp. 686–706.
- [25] Vigliani A., *Lectures on rotordynamics*, CLUT, Torino, 2010.
- [26] Earnshaw S., “On the nature of the molecular forces wich regulate the constitution of the luminiferous ether”, *Transaction of Cambridge Philisophical Society*, 7(116), 1842, pp. 97-112.
- [27] Bonisoli E., “LUPOS: Lumped Parameters Open Source FEM code”, Tutorial v.2019-08-16, Politecnico di Torino, Department of Mechanical and Aerospace Engineering, 2019.
- [28] Cowper G.R., “The shear coefficient in Timoshenko’s beam theory”, *Transaction of ASME, Journal of Applied Mechanics*, 33(2), 1966, pp. 335-340.
- [29] Branagan M., *Rotordynamic Analyses using Finite Element Method*, Master Thesis, School of Engineering and Applied Science, University of Virginia, 2014.

Acknowledgments

I would like to express my deep gratitude to all the people who made this project possible. First of all my family, for supporting me like the magnetic bearings do with the rotating rotor, showing me the path without holding me back. A special mention goes to my British speaking family, for their affection from overseas. Thanks to ‘those of the vermouth’ for sharing this experience with me.

Mega, always by my side.

This is not the end of an adventure, it is just the beginning.